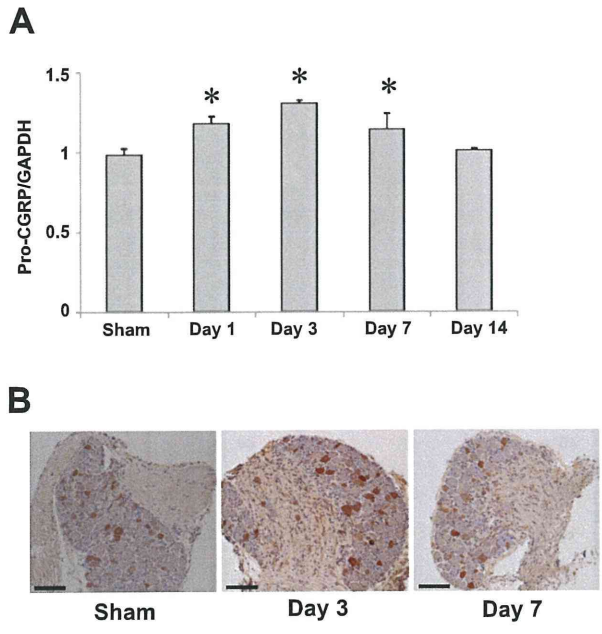

Fig. 4. Expression of CGRP in the lumbar dorsal root ganglia (DRG) and the ischemic tissue following hindlimb ischemia. *A*: ipsilateral lumbar DRG were excised from the spinal cord 1 and 3, 7, and 14 days after the left femoral artery ligation. Data are means ± SE from 4 mice/group. $^*P < 0.05$ vs. sham-operated mice. *B*: typical appearance of DRG sections stained with CGRP. The immunoreactivity with CGRP in the DRG neurons and nerve fibers was enhanced 3 days after the induction of hindlimb ischemia. Bars indicate 100 μm. *C*: representative photographs of ischemic tissues stained with CGRP 7 days after hindlimb ischemia. *Top*, $CGRP^{+/+}$; bottom, $CGRP^{-/-}$. Bars indicate 100 μm.

blasts (Fig. 7). Real-time RT-PCR analysis on CGRP receptors revealed that transcripts encoding CRLR, a subunit of CGRP1, were detected on both HUVECs and fibroblasts. By contrast, CTRa, a subunit of CGRP2, was not detected in either HUVECs or fibroblasts. The mRNA expression of RAMP-1, a common subunit of CGRP receptors, was present, but their levels were weak.

Blockade of the CGRP receptor impaired ischemia-induced revascularization. We also investigated the effects of continuous infusion of a CGRP antagonist, CGRP8–37, using miniosmotic pumps, on ischemia-induced revascularization (Fig. 8). The ratio of ischemic to nonischemic flow 7 and 14 days after surgery was 36 and 12% less, respectively, in mice treated with CGRP8–37 compared with that of mice treated with vehicle (Fig. 8*A*). Capillary density in CGRP8–37-treated mice was lower (41% decrease) than that in vehicle-treated mice (Fig. 8*B*). In vivo microscopic studies demonstrated that the functional capillary density in the perifemoral and muscular regions 7 days after the induction of ischemia was reduced (by 46 and 44%, respectively) (Fig. 8*C*). These findings indicate that the results from $CGRP^{-/-}$ are essentially the same as those from mice treated with the CGRP antagonist.

Downregulated expression of growth factors in CGRP8–37-treated mice. We determined the mRNA expression levels of proangiogenic factors by real-time RT-PCR. Three days after the hindlimb ischemia, the levels of expression for CD31, VEGF-A, bFGF, and TGF-β in CGRP8–37-treated mice were decreased by 50, 67, 46, and 53%, respectively, compared with vehicle-treated mice (Fig. 9).

DISCUSSION

CGRP is a 37-amino acid neuropeptide produced by tissue-specific alternative splicing of the primary transcript of the calcitonin/CGRP gene (3). Although cardiovascular phenotypes were studied (13, 20), little attention was focused on the contribution of CGRP to angiogenesis in response to ischemia in CGRP null mice. The present study showed that CGRP accelerated vascular regeneration in the murine ischemic model by enhancing the expression of proangiogenic growth factors (Figs. 1, 3, and 5). Impaired blood flow recovery from ischemia and reduced capillary density in CGRP knockout mice provide evidence that CGRP upregulates ischemia-induced angiogenesis. In vivo microscopic observation revealed that revascularization was observed in the ischemic tissues and that that in CGRP knockout mice was suppressed. The finding that infusion of a CGRP antagonist, CGRP8–37, suppressed angiogenesis supports the results from CGRP knockout mice (Fig. 8). These results suggest that CGRP, which is synthesized in the neuronal systems, enhances angiogenesis in this model. Thus, the blood flow recovery from ischemia that is dependent on angiogenesis may be facilitated by endogenous CGRP.

Within the nervous system, CGRP has been detected in spinal cord motor neurons, DRG, and motor nerve endings (30). Sensory nerves can be activated by a variety of physical and chemical stimuli (6). Upon induction of inflammation, CGRP is upregulated, and pro-CGRP mRNA levels in the DRG that innervate the sites of inflammation rise (31). In the current study, pro-CGRP mRNA levels in the DRG (L_1-L_5) were upregulated during the evolution of revascularization in response to ischemia (Fig. 4). The pro-CGRP expression in the DRG was correlated with the expression of CGRP in the DRG as well as in the nerves of the ischemic limbs. These findings indicate that hindlimb ischemia enhances the expression of pro-CGRP in the DRG that innervated the area affected by ischemia and that CGRP is synthesized in the neuronal systems and is delivered to the periphery of the nerves innervating the sites of revascularization. The effects of a CGRP antagonist and of CGRP gene disruption on revascularization suggest that CGRP release from the peripheral nerve endings during hindlimb ischemia may stimulate the proangiogenic activities. It has been shown that myocardial ischemia-reperfusion results in

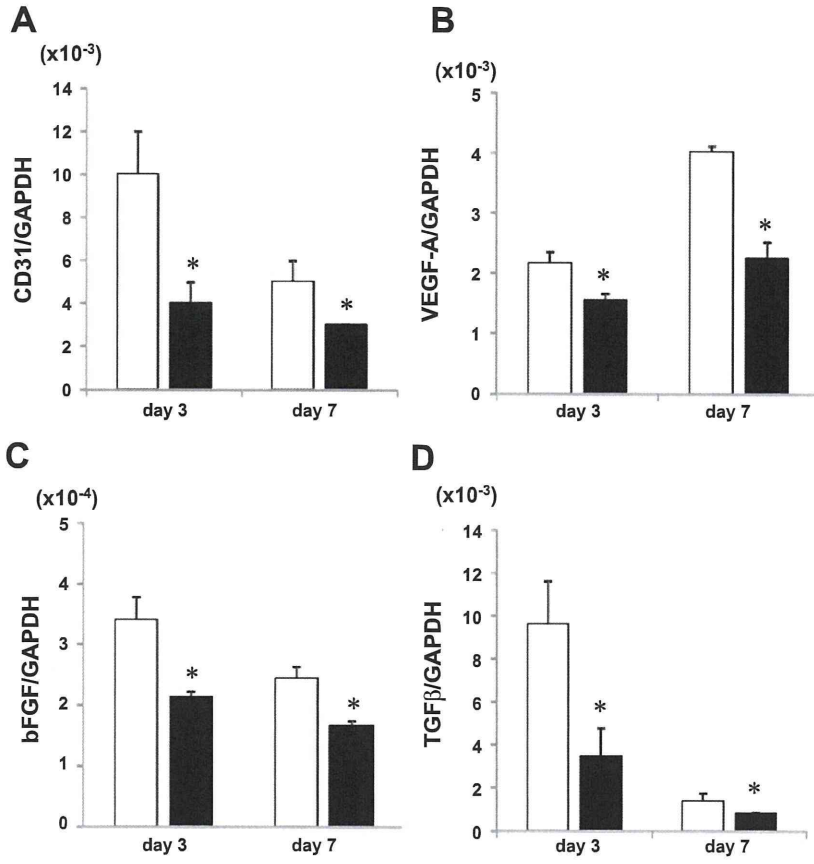

Fig. 5. Expression of mRNA for growth factors in the ischemic tissue following hindlimb ischemia. Expression of growth factors, including CD31 (*A*), vascular endothelial growth factor (VEGF)-A (*B*), basic fibroblast growth factor (bFGF, *C*), and transforming growth factor-β (TGF-β, *D*) in ischemic tissue 3 and 7 days after the induction of ischemia. Real-time RT-PCR was performed as described in MATERIALS AND METHODS. Expression was normalized against that of glyceraldehyde-3-phosphate dehydrogenase (GADPH). Data are means ± SE from 6 mice/group. Open bar, $CGRP^{+/+}$; filled bar, $CGRP^{-/-}$. $^*P < 0.05$ vs. $CGRP^{+/+}$.

the release of CGRP from sensory nerve terminals in rodents (22). The tissues exposed to ischemia might produce various metabolites, including bradykinin, reactive oxygen species, protons, and arachidonate metabolites, some of which may activate sensory C-fibers to release CGRP (11). Moreover, immunoelectron microscopic studies reveal that CGRP-immunoreactive gold particles are localized on the ECs (7, 9). Thus, in addition to the DRG, ECs themselves could synthesize CGPR during hindlimb ischemia.

It was reported that one of the sensory neuropeptides, substance P, has a proangiogenic activity (10); however, the details of the mechanism underlying enhanced angiogenesis were not precisely studied. In the present experiment, another neuropeptide, CGRP, was found to facilitate ischemia-induced angiogenesis by enhancing the expression of proangiogenic factors, including CD31, VEGF-A, bFGF, and TGF-β, in the ischemic tissues where angiogenesis was predominantly observed (Fig. 5).

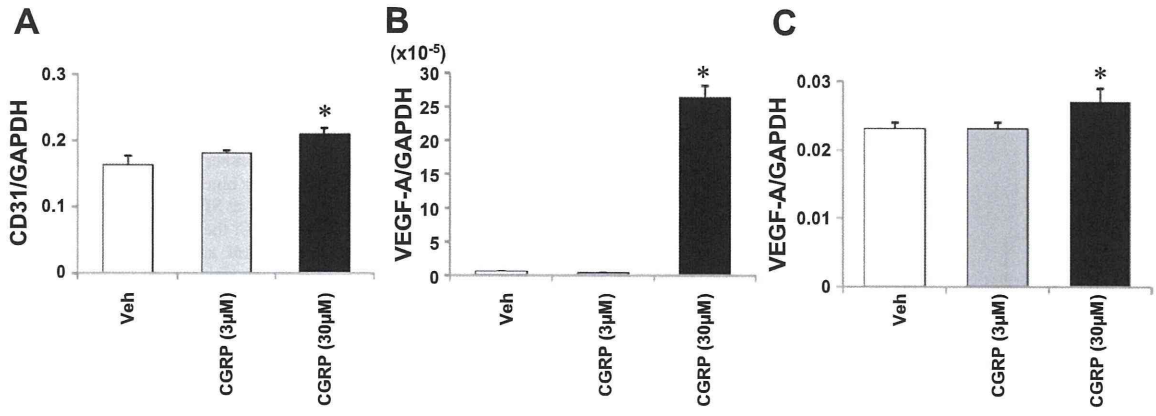

Fig. 6. Expression of growth factors in human umbilical vein endothelial cells (HUVECs) and fibroblasts stimulated with CGRP. The mRNA expression of CD31 (*A*) and VEGF-A (*B*) in HUVECs and of VEGF-A (*C*) in L929 fibroblasts was tested 6 h after CGRP (3 and 30 μM) or vehicle (PBS) with real-time RT-PCR. Expression was normalized against that of GADPH. Data are means ± SE from 3 independent experiments. $^*P < 0.05$ vs. vehicle (Veh).

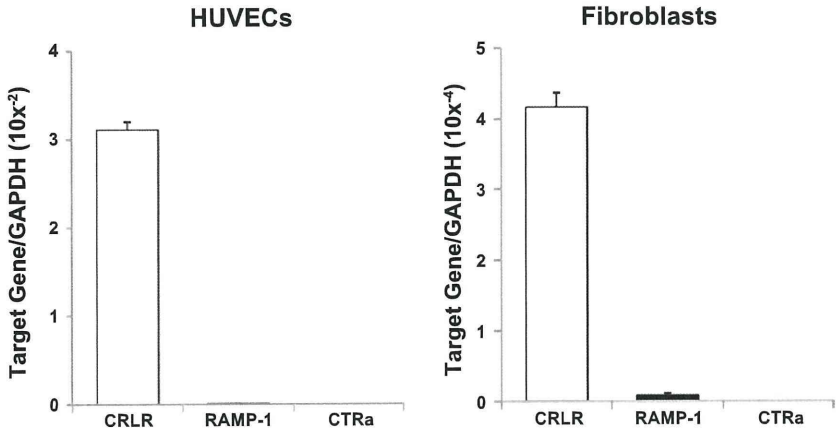

Fig. 7. Expression of CGRP receptors in HUVECs and L929 fibroblasts. The mRNA expression of calcitonin receptor-like receptor (CRLR), calcitonin receptor (CTR) a, and receptor activity-modifying protein (RAMP)-1 in HUVECs and L929 fibroblasts was determined by real-time RT-PCR analysis. Data are means ± SE from 3 independent experiments.

The current study also demonstrates that CGRP exhibits proangiogenic activity by enhancing the expression of VEGF and CD31 in HUVECs and the expression of VEGF in fibroblasts (Fig. 6). Consistent with this result, our recent report (29) demonstrated that tumor growth and tumor-associated angiogenesis are inhibited in CGRP$^{-/-}$ mice implanted with Lewis lung carcinoma cells, which is associated with reduced VEGF expression in tumor tissues. In addition, we have shown that CGRP enhances tube formation activity in a coculture system using HUVECs and fibroblasts (29). The capillary-like tube formation elicited by CGRP is blunted by VEGF antibody (29). Moreover, we reported that VEGF is involved in hindlimb ischemia-induced angiogenesis because an antibody against VEGF inhibited blood flow recovery from hindlimb ischemia (2), suggesting that VEGF may work as a downstream molecule. The other proangiogenic factors, such as bFGF and TGF-β, may also participate in CGRP-mediated angiogenesis during hindlimb ischemia. Because CGRP is a potent vasodilator, its vasodilatory activity in addition to its proangiogenic activity would increase blood flow during hindlimb ischemia.

The status of CGRP receptor is critical to understand the pathophysiological roles of endogenous CGRP. The results of RT-PCR of CGRP receptors revealed the detection of the expression of CRLR mRNA, a subunit of CGRP1, in cultured HUVECs and fibroblasts. By contrast, CTRa, a subunit of CGRP2, was not detected. RAMP-1 mRNA, a common subunit of CGRP receptors, was present, but their level of expres-

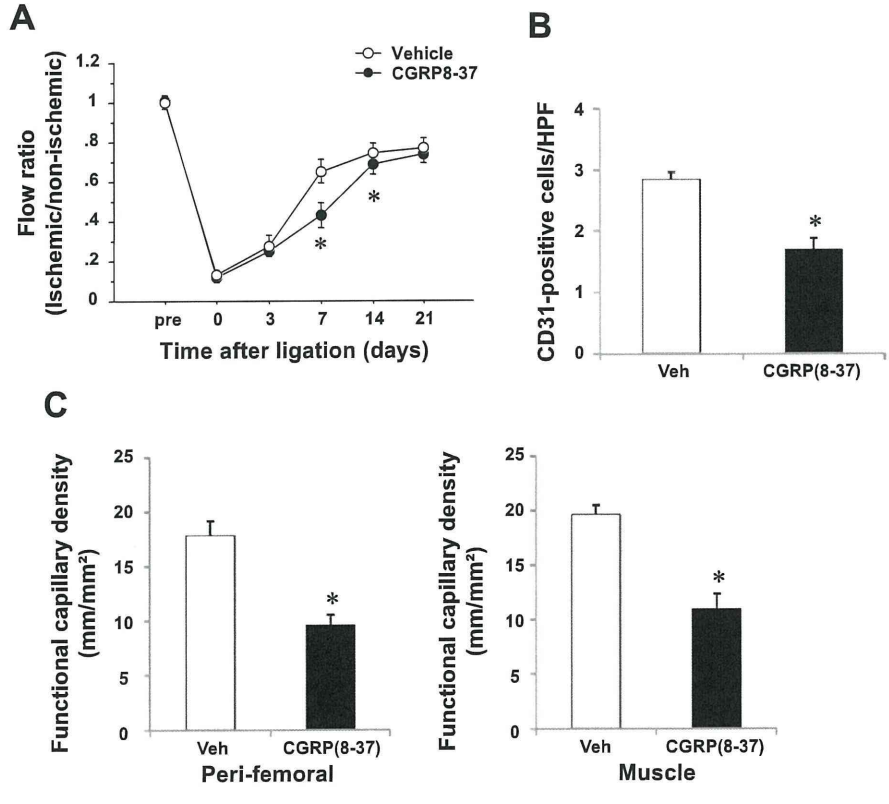

Fig. 8. Effects of continuous subcutaneous infusion of the CGRP antagonist, CGRP8–37, on revascularization in response to hindlimb ischemia. *A*: time course of ischemic/nonischemic perfusion ratios in C57Bl/6 mice treated with CGRP8–37 or vehicle (physiological saline). Blood flow was assessed by LDF and was determined before (pre), immediately after (0), and 3, 7, 14, and 21 days after the left femoral artery ligation. Results are expressed as a ratio of the left (ischemic) to right (nonischemic) limb perfusion rate. Data are means ± SE from 6 mice/group. *$P < 0.05$ vs. vehicle. *B*: quantitative analysis of capillary density expressed in terms of the number of CD-31-positive cells/HPF at 7 days after hindlimb ischemia. Data are expressed as means ± SE from 6 mice/group. *$P < 0.05$ vs. vehicle. *C*: the functional capillary density in the perifemoral and muscular regions in ischemic limbs was determined using in vivo microscopic methods 7 days after the hindlimb ischemia. Data are means ± SE from 6 mice/group. *$P < 0.05$ vs. vehicle.

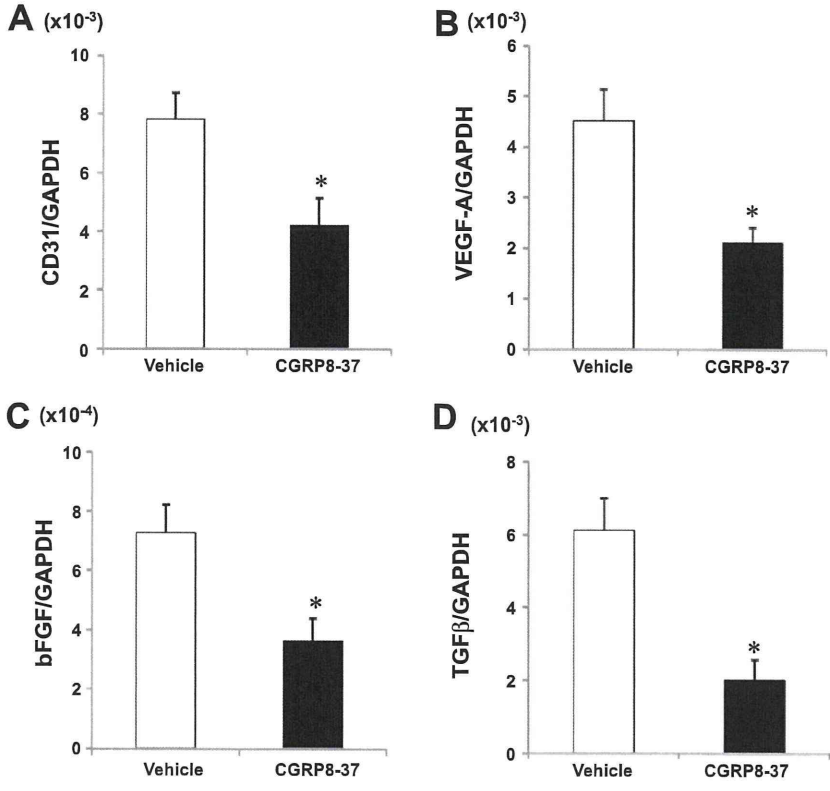

Fig. 9. Effect of CGRP8–37 on the expression of growth factors in ischemic tissue following hindlimb ischemia. At 3 days after surgery, CGRP8–37 reduced the mRNA expression of CD31 (*A*), VEGF-A (*B*), bFGF (*C*), and TGF-β (*D*). Real-time RT-PCR was performed as described in MATERIALS AND METHODS. Expression was normalized against that of GADPH. All data are means ± SE from 6 mice/group. $^*P < 0.05$ vs. vehicle.

sion was weak. These results suggest that CGRP1 in ECs and fibroblasts has a significant role in facilitating the revascularization during hindlimb ischemia. In fact, in the sponge model (29) as well as in the current model, the angiogenic reaction was inhibited by CGRP-(8–37), a CGRP1 antagonist. The mechanisms underlying that CGRP exerts its angiogenic activity through CGRP1 receptor signaling on ECs and fibroblasts are uncertain. However, CGRP1 signaling is known to activate adenylate cyclase to increase intracellular cAMP levels (6). We reported that increased cAMP through activation of adenylate cyclase/protein kinase A results in VEGF expression and facilitates angiogenesis in vivo (1). These results indicate that CGRP enhances the expression of VEGF through cAMP elevation followed by CGRP1 receptor stimulation. CGRP also is capable of activating phosphatidylinositol-3 kinase/protein kinase B and mitogen-activated protein kinase (MAPK) pathways in cultured human embryonic kidney cells via CGRP1 (27) and in cultured ECs via CRLR (25). Moreover, CGRP upregulates the expression of VEGF in human HaCaT keratinocytes by activation of extracellular signal-regulated kinase 1/2 MAPK (32). Further studies are necessary to clarify the molecular mechanisms by which CGRP regulates the angiogenic factors through activation of intrasignaling pathways.

During the prenatal development, the expression of CGRP in the lumber DRG first appears on *embryonic day 16* in mice (12). On *embryonic day 18*, abundant DRG neurons expressing CGRP are observed. These findings indicate that CGRP develops well in the late stages of gestation. Therefore, it is plausible that CGPR may not be critical for vascular formation during embryogenesis. Indeed, $CGRP^{-/-}$ mice have normal general development and display no defective vascular formation (26), indicating that CGRP plays a minimal role in prenatal angiogenesis and in postnatal or physiological vessel growth. Consistent with this, the current study showed that blood flow levels were same between $CGRP^{-/-}$ and $CGRP^{+/+}$ before the induction of hindlimb ischemia.

Although CGRP plays a critical role in revascularization in response to hindlimb ischemia, the proangiogenic activity as indicated by growth factor expression and capillary density mainly exhibited within 7 days after induction of hindlimb ischemia. The blood perfusion in $CGRP^{-/-}$ mice was restored to the similar levels of WT mice 3 wk after hindlimb ischemia. The short-term duration of its effect on proangiogenic activity is supported by the finding that expression of precursor-CGRP is transiently upregulated during revascularization in response to hindlimb ischemia. This suggests that CGRP is involved in the stimulation of revascularization during the early phase of ischemia-induced angiogenesis, even though the CGRP gene is disrupted. These results also suggest that other neuropeptides, including substance P and adrenomedulin, could be involved in revascularization after hindlimb ischemia.

In conclusion, we demonstrated that CGRP has a role in enhancing blood flow recovery during hindlimb ischemia. CGRP8–37 can block the CGRP-dependent enhancement of angiogenesis. Upregulation of the expression of proangiogenic growth factors was associated with enhanced blood flow recovery and revascularization. These results indicate that endogenous CGRP, which is possibly released from the neuronal systems, has a significant role in ischemia-associated angiogenesis. Targeting of CGRP may provide a promising method for controlling pathophysiological angiogenesis.

ACKNOWLEDGMENTS

We thank Michiko Ogino, Mieko Hamano, and Akira Nara for technical assistance. We express our thanks to BioEdit for correcting the English of this manuscript.

GRANTS

This work was supported by grants from the Ministry of Education, Culture, Sports, Science, and Technology (Research Grants 20659037 and 21591761, High-Tech Research Center Grant, Academic Frontier Project Grant, and The 21st Century COE Program Grant), the Integrative Research Program of the Graduate School of Medical Science, Kitasato University, and the Parents' Association Grant of Kitasato University School of Medicine.

DISCLOSURES

No conflicts of interest are declared by the authors.

REFERENCES

1. **Amano H, Ando K, Minamida S, Hayashi I, Ogino M, Yamashina S, Yoshimura H, Majima M.** Adenylate cyclase/protein kinaseA signaling pathway enhances angiogenesis through induction of vascular endothelial growth factor in vivo. *Jpn J Pharmacol* 87:181–188, 2001.
2. **Amano H, Hackett NR, Rafii S, Crystal RG.** Thrombopoietin gene transfer-mediated enhancement of angiogenic responses to acute ischemia. *Circ Res* 97: 337–345, 2005.
3. **Amara SG, Jonas V, Rosenfeld MG, Ong ES, Evans RM.** Alternative RNA processing in calcitonin gene expression generates mRNAs encoding different polypeptide products. *Nature* 298: 240–244, 1982.
4. **Arai K, Ohno T, Saeki T, Mizuguchi S, Kamata K, Hayashi I, Saigenji K, Murata T, Narumiya S, Majima M.** Endogenous prostaglandin I2 regulates the neural emergency system through release of calcitonin gene related peptide. *Gut* 52: 1242–1249, 2003.
5. **Boku K, Ohno T, Saeki T, Hayashi H, Hayashi I, Katori M, Murata T, Narumiya S, Saigenji K, Majima M.** Adaptive cytoprotection mediated by prostaglandin I(2) is attributable to sensitization of CRGP-containing sensory nerves. *Gastroenterology* 120: 134–143, 2001.
6. **Brain SD, Grant AD.** Vascular Actions of Calcitonin Gene-Related Peptide and Adrenomedullin. *Physiol Rev* 84: 903–934, 2003.
7. **Cai WQ, Dikranian K, Bodin P, Turmaine M, Burnstock G.** Colocalization of vasoactive substances in the endothelial cells of human umbilical vessels. *Cell Tissue Res* 274: 533–538, 1993.
8. **Carmeliet P.** Mechanisms of angiogenesis and arteriogenesis. *Nat Med* 6: 389–395, 2000.
9. **Doi Y, Kudo H, Nishino T, Kayashima K, Kiyonaga H, Nagata T, Nara S, Morita M, Fujimoto S.** Synthesis of calcitonin gene-related peptide (CGRP) by rat arterial endothelial cells. *Histol Histopathol* 16: 1073–1079, 2001.
10. **Fan TP, Hu DE, Guard S, Gresham GA, Watling KJ.** Stimulation of angiogenesis by substance P and interleukin-1 in the rat and its inhibition by NK1 or interleukin-1 receptor antagonists. *Br J Pharmacol* 110: 43–49, 1993.
11. **Franco-Cereceda A, Saria A, Lundberg JM.** Differential release of calcitonin gene-related peptide and neuropeptide Y from the isolated heart by capsaicin, ischaemia, nicotine, bradykinin and ouabain. *Acta Physiol Scand* 135: 173–187, 1989.
12. **Funakoshi K, Goris RC, Kadota T, Atobe Y, Nakano M, Kishida R.** Prenatal development of peptidergic primary afferent projections to mouse lumbosacral autonomic preganglionic cell columns. *Dev Brain Res* 144: 107–119, 2003.
13. **Gangula PR, Zhao H, Supowit SC, Wimalawansa SJ, Dipette DJ, Westlund KN, Gagel RF, Yallampalli C.** Increased blood pressure in alpha-calcitonin gene-related peptide/calcitonin gene knockout mice. *Hypertension* 35: 470–475, 2000.
14. **Haegerstrand A, Dalsgaard CJ, Jonzon B, Larsson O, Nilsson J.** Calcitonin gene-related peptide stimulates proliferation of human endothelial cells. *Proc Natl Acad Sci USA* 87: 3299–3303, 1990.
15. **Holzer P.** Neural emergency system in the stomach. *Gastroenterology* 114: 823–839, 1998.
16. **Huang R, Karve A, Shah I, Bowers MC, DiPette DJ, Supowit SC, Abela GS.** Deletion of the mouse alpha-calcitonin gene-related peptide gene increases the vulnerability of the heart to ischemia-reperfusion injury. *Am J Physiol Heart Circ Physiol* 294: H1291–H1297, 2008.
17. **Kato S, Amano H, Ito Y, Eshima K, Aoyama N, Tamaki H, Sakagami H, Satoh Y, Izumi T, Majima M.** Effect of erythropoietin on angiogenesis with the increased adhesion of platelets to the microvessels in the hind-limb ischemia model in mice. *J Pharmacol Sci* 112: 167–175, 2010.
18. **Katoh H, Hosono K, Ito Y, Suzuki T, Ogawa Y, Kubo H, Kamata H, Mishima T, Tamaki H, Sakagami H, Sugimoto Y, Narumiya S, Watanabe M, Majima M.** COX-2 and prostaglandin EP3/EP4 signaling regulate the tumor stromal proangiogenic microenvironment via CXCL12-CXCR4 chemokine systems. *Am J Pathol* 176: 1469–1483, 2010.
19. **Kobayashi T, Tahara Y, Matsumoto M, Iguchi M, Sano H, Murayama T, Arai H, Oida H, Yurugi-Kobayashi T, Yamashita JK, Katagiri H, Majima M, Yokode M, Kita T, Narumiya S.** Roles of thromboxane A (2) and prostacyclin in the development of artherosclerosis in apo-E deficient mice. *J Clin Invest* 114: 784–794, 2004.
20. **Lu JT, Son YJ, Lee J, Jetton TL, Shiota M, Moscoso L, Niswender KD, Loewy AD, Magnuson MA, Sanes JR, Emeson RB.** Mice lacking alpha-calcitonin gene related peptide exhibit normal cardiovascular regulation and neuromuscular development. *Mol Cell Neurosci* 14: 99–120, 1999.
21. **Mantyh PW, Clohisy DR, Koltzenburg M, Hunt SP.** Molecular mechanisms of cancer pain. *Nat Rev Cancer* 2: 2001–2209, 2002.
22. **Manzini S, Perretti F, De Benedetti L, Pradelles P, Maggi CA, Geppetti P.** A comparison of bradykinin- and capsaicin-induced myocardial and coronary effects in isolated perfused heart of guinea-pig: involvement of substance P and calcitonin gene-related peptide release. *Br J Pharmacol* 97: 303–312, 1989.
23. **Miller G.** Developmental biology, Nerves tell arteries to make like a tree. *Science* 296: 2121–2123, 2002.
24. **Mukouyama YS, Anderson DJ.** Sensory nerves determine the pattern of arterial differentiation and blood vessel branching in the skin. *Cell* 109: 693–705, 2002.
25. **Nikitenko LL, Blucher N, Fox SB, Bicknell R, Smith DM, Rees MC.** Adrenomedullin and CGRP interact with endogenous calcitonin-receptor-like receptor in endothelial cells and induce its desensitisation by different mechanisms. *J Cell Sci.* 119: 910–922, 2006.
26. **Oh-hashi Y, Kurihara H.** Elevated sympathetic nervous activity in mice deficient in alphaCGRP. *Circ Res* 11: 983–990, 2001.
27. **Parameswaran N, Disa J, Spielman WS, Brooks DP, Nambi P, Aiyar N.** Activation of multiple mitogen-activated protein kinases by recombinant calcitonin gene-related peptide receptor. *Eur J Pharmacol* 389: 125–130, 2000.
28. **Saeki T, Ohno T, Kamata K, Arai K, Mizuguchi S, Katori M, Saigenji K, Majima M.** Mild irritant prevents ethanol-induced gastric mucosal microcirculatory disturbances through actions of calcitonin gene-related peptide and PGI2 in rats. *Am J Physiol Gastrointest Liver Physiol* 286: G68–G75, 2004.
29. **Toda M, Suzuki T, Hosono K, Hayashi I, Hashiba S, Onuma Y, Amano H, Kurihara Y, Kurihara H, Okamoto H, Hoka S, Majima M.** Neuronal system-dependent facilitation of tumor angiogenesis and tumor growth by calcitonin gene-related peptide. *Proc Natl Acad Sci USA* 105: 13550–13555, 2008.
30. **Wimalawansa SJ.** Calcitonin gene-related peptide and its receptors: molecular genetics, physiology, pathophysiology, and therapeutic potentials. *Endocr Rev* 17: 533–585, 1996.
31. **Xu P, Van Slambrouck C, Berti-Mattera L, Hall AK.** Activin induces tactile allodynia and increases calcitonin gene-related peptide after peripheral inflammation. *J Neurosci* 25: 9227–9235, 2005.
32. **Yu XJ, Li CY, Wang KY, Dai HY.** Calcitonin gene-related peptide regulates the expression of vascular endothelial growth factor in human HaCaT keratinocytes by activation of ERK1/2 MAPK. *Regul Pept* 137: 134–139, 2006.

Development 138, 4763-4776 (2011) doi:10.1242/dev.068023

Angiogenic morphogenesis driven by dynamic and heterogeneous collective endothelial cell movement

Satoshi Arima*, Koichi Nishiyama*,†, Toshiyuki Ko, Yuichiro Arima, Yuji Hakozaki, Kei Sugihara, Hiroaki Koseki, Yasunobu Uchijima, Yukiko Kurihara and Hiroki Kurihara

SUMMARY

Angiogenesis is a complex process, which is accomplished by reiteration of modules such as sprouting, elongation and bifurcation, that configures branching vascular networks. However, details of the individual and collective behaviors of vascular endothelial cells (ECs) during angiogenic morphogenesis remain largely unknown. Herein, we established a time-lapse imaging and computer-assisted analysis system that quantitatively characterizes behaviors in sprouting angiogenesis. Surprisingly, ECs moved backwards and forwards, overtaking each other even at the tip, showing an unknown mode of collective cell movement with dynamic 'cell-mixing'. Mosaic analysis, which enabled us to monitor the behavior of individual cells in a multicellular structure, confirmed the 'cell-mixing' phenomenon of ECs that occurs at the whole-cell level. Furthermore, an in vivo EC-tracking analysis revealed evidence of cell-mixing and overtaking at the tip in developing murine retinal vessels. In parametrical analysis, VEGF enhanced tip cell behavior and directed EC migration at the stalk during branch elongation. These movements were counter-regulated by EC-EC interplay via γ-secretase-dependent Dll4-Notch signaling, and might be promoted by EC-mural cell interplay. Finally, multiple regression analysis showed that these molecule-mediated tip cell behaviors and directed EC migration contributed to effective branch elongation. Taken together, our findings provide new insights into the individual and collective EC movements driving angiogenic morphogenesis. The methodology used for this analysis might serve to bridge the gap in our understanding between individual cell behavior and branching morphogenesis.

KEY WORDS: Angiogenesis, Time-lapse imaging, Collective cell movement, Mouse

INTRODUCTION

Morphogenetic cell movement gives rise to various types of geometry observed in the living world. The processes are diverse, and recently the notion of collective cell movement has increasingly become a focus of research. Known collective cell movements include branching morphogenesis of the mammary gland, cluster movement of detached cancer cells, border cell migration in *Drosophila* eggs and lateral line primordium migration in zebrafish (Montell, 2008; Friedl and Gilmour, 2009).

Angiogenesis is a multicellular phenomenon whereby new blood vessels emerge from an existing vascular network in developmental and (patho)physiological contexts. Current understanding of angiogenesis encompasses tip cell selection by lateral inhibition, elongation, branching, anastomosis, vessel stabilization and lumen formation (Holderfield and Hughes, 2008; De Smet et al., 2009). Endothelial cell (EC) signaling involving the vascular endothelial growth factor (VEGF)-receptor (VEGFR), angiopoietin-Tie2 and Ephrin-Eph pathways has been intensively elucidated its role in these events (Armulik et al., 2005; Holderfield and Hughes, 2008; Gaengel et al., 2009). In addition, the interaction between ECs and mural cells (MCs), including vascular smooth muscle cells and pericytes, has also been implicated in the maintenance of the angiogenic process for appropriate organization (Hellstrom et al., 2001; Lafleur et al., 2001; Armulik et al., 2005; Gaengel et al., 2009; Liu et al., 2009).

Department of Physiological Chemistry and Metabolism, Graduate School of Medicine, The University of Tokyo, 7-3-1, Hongo, Bunkyo-ku, Tokyo, 113-0033, Japan.

*These authors contributed equally to this work
†Author for correspondence (nkanako@bio.m.u-tokyo.ac.jp)

Accepted 22 August 2011

Despite the extensive past studies, how the spatiotemporal regulation of molecules affects morphogenetic cell movement and what type of collective cell movement is involved in angiogenesis remain elusive, largely owing to the lack of a stable methodology for visualizing and assessing EC movements during angiogenesis. It is only recently that research has begun to focus on and assess real-time EC behavior during these processes (Murakami et al., 2006; Perryn et al., 2008; Vitorino and Meyer, 2008). In order to clarify the relationship between individual cell movements and angiogenic morphology, and to dissect the underlying molecular and cellular mechanisms, we first established a system in which dynamic cell behavior is visualized using time-lapse microscopy and set out to identify patterns of cellular behavior in an angiogenesis model through computational data processing. Surprisingly, cell movements were far more dynamic and heterogeneous in movement than previously thought. In elongating branches, ECs moved changing their relative positional relationships to each other at the tip. This 'cell-mixing' phenomenon was also confirmed in developing murine retinal vessels in vivo.

We further established a computer-assisted quantitative analysis system with which we can assess molecular and cellular mechanisms underlying complex EC movements. After validation of this system by analyzing the angiogenic effect of VEGF, we applied it to determining the role of Notch-related signaling in angiogenesis.

Recently, roles of Delta-like 4 (Dll4)-Notch signaling in angiogenesis have been demonstrated by a series of reports (Ridgway et al., 2006; Hellstrom et al., 2007; Siekmann and Lawson, 2007; Suchting et al., 2007). Murine retina heterozygous for a null mutation of the *Dll4* gene showed excessive branching and this was recapitulated by administering a γ-secretase inhibitor,

DAPT. Zebrafish in which Dll4 signaling was abolished using morpholino knockdown had increased migratory cells in intersomitic vessels. Blockade of Dll4 resulted in deregulated angiogenesis with a rather paradoxical reduction in tumor size. All of these findings have been attributed to a signaling cascade in which Dll4, by acting through Notch1, regulates tip cell differentiation. However, reports focusing on how individual EC movements are integrated into vascular morphology remain scarce.

The present analysis revealed that EC-EC interplay via Dll4-Notch signaling counter-regulated not only VEGF-induced tip cell behavior but also directed migration of stalk cells. In addition, EC-MC interplay might positively regulate EC behaviors, implying a novel role for MCs in the early stage of angiogenesis.

These findings, along with our time-lapse quantitative analyses, provide new insights into EC movements during angiogenesis, and the imaging and analysis system that we established should prove to be a powerful tool for linking individual cellular behaviors, molecular events and morphogenetic collective cell movements.

MATERIALS AND METHODS

Animals

ICR mice were purchased from Charles River Laboratories Japan and used in all experiments except for those on mice carrying the *Ednrd*^{Egfp} (*EGFP*-knock-in) allele (Asai et al., 2010). All animal experiments were reviewed and approved by The University of Tokyo Animal Care and Use Committee and were performed in accordance with the institutional guidelines.

Antibodies

The following antibodies were used: rat anti-CD31 (BD Pharmingen); rabbit anti-Dll4 and rat anti-platelet-derived growth factor receptor β (PDGFRβ) (Biolegend); rabbit anti-GFP (MBL); rabbit anti-NG2 and rabbit anti-phospho-histone H3 (PH3) (Millipore); and rat anti-PDGFRβ for neutralization (a gift from Dr Shin-ichi Nishikawa, RIKEN, Kobe, Japan).

Aortic ring assay and time-lapse live imaging

The aortic ring assay was performed as previously described (Blacher et al., 2001). Aortic rings were embedded in type I collagen gel (Nitta Gelatin) on eight-well chambered coverglasses (Nunc) and were cultured in medium-199 containing 5% FCS, 10 μg/ml streptomycin, 100 units/ml penicillin and 50 ng/ml human recombinant VEGF (R&D) (complete medium).

Time-lapse live imaging was started on the 5th or 6th day of the assay. For EC tracking, we labeled cells with SYTO-16 or SYTO-61 (0.1 μg/ml, Molecular Probes). Dynamic cell behavior was analyzed using a confocal laser scanning microscope (FluoView FV10i Olympus). Time-lapse live images were taken at 8-10 μm intervals for the *z*-axis every 15 minutes over 36 hours (10× 0.4 NA air objective), and for some assays, at 3 μm intervals every 5-7 minutes over 5-12 hours (60× 1.2 NA water-immersion objective). Obtained images were processed with analysis software FLUOVIEW (Olympus).

For mosaic analysis, the aortic ring was infected with adenovirus carrying EGFP (1×10^5 p.f.u./ml) (a gift from Dr Hideyuki Sakoda, The University of Tokyo, Japan) before cultivation. If needed, cells were incubated with 5 μg/ml of BS-1 lectin to visualize ECs.

Chemical interventions

To examine the effect of VEGF on sprouting angiogenesis, culture media were replaced with medium-199 containing 5% FCS, 10 μg/ml streptomycin, 100 units/ml penicillin and the indicated dose of VEGF 3 hours prior to time-lapse imaging. To inhibit Dll4-Notch signaling, sprouts were pre-treated with 50 μg/ml anti-Dll4-Ab (Yamanda et al., 2009) or 3 μM N-[N-(3,5-difluorophenacetyl-L-alanyl)]-S-phenylglycine t-butyl ester (DAPT, Sigma), a γ-secretase inhibitor, 24 hours prior to time-lapse live imaging. For morphological analysis, anti-Dll4-Ab or DAPT was added throughout the assay. To inhibit the PDGFRβ signal, cells were treated with anti-PDGFRβ-Ab (10 μg/ml) in complete medium throughout the assay (Uemura et al., 2002).

In vivo EC-tracking analysis

To label ECs of the retinal vasculature intravascularly, 3-5 μg of fluorescent-conjugated BS-1 lectin (Sigma) was injected into the cardiac chamber of neonatal mice beginning on postnatal day 1 using glass capillary pipettes. Retinas were obtained at the indicated time after the injection.

In silico analysis

Cell tracking, data extraction and data analysis were carried out using ImageJ, MTrackJ and MATLAB.

Cell tracking

Nuclei of each EC were manually selected, and whenever two or more nuclei overlapped, general rules were applied to define the next points of the current track: (1) when there is obvious flow of cells in one direction, a cell is likely to move on that axis either anterograde or retrograde, albeit with some deviation; (2) in the setting of (1) and when there are two or more candidate axes, cells are prone to move on their previous axis and in their prior direction; (3) in the setting of (2), when there are more than two candidate positions for the next slice, either the nearest possible and/or the one most likely regarding the previous velocity is chosen; and (4) normally, cells avoid bumping into each other by fine-tuning their velocities and directions.

Definitions

The term 'tip cells' refers to 'cells at the tip of a certain time point'. The other, non-tip cells, were termed 'stalk cells'. A branch was defined as a multicellular protrusion with more than two ECs. A 'junction' was defined as a point of divergence, juncture or intersection of several vessels, and a 'stalk' was the region distal to a junction. The area of analysis was defined by setting four coordinates that surround all nuclei in a stalk or a junction. The latter was set to exclude as the cells of distal stalks as much as possible.

The axis and direction of elongation (elongation vector, $\boldsymbol{E}$) was defined as $\boldsymbol{E}=\boldsymbol{r}(end)-\boldsymbol{r}(0)$, where $\boldsymbol{r}(t)$ stood for the coordinates of the tip at $time=t$ ('end' stands for the last observed time point). When a branch sprouted out after the start, $t=0$ meant the start of elongation and thus of the sprouting event. To this end, the tip was tracked independently. The coordinates of each cell were calculated by orthogonal projection to the axis of elongation. Therefore, $e(i,t)=dot[\boldsymbol{E},(\boldsymbol{r}(i,t)-\boldsymbol{e}0)]/|\boldsymbol{E}|$, where $e(i,t)$ stood for the one-dimensional coordinates of a cell with an $ID=i$ at $time=t$ obtained by orthogonal projection. $\boldsymbol{r}(i,t)$ was the original coordinates of i-th cell at $time=t$. 0 on this axis meant the initial coordinates of the tip ($\boldsymbol{e}0$) projected to the elongation vector, and $dot[\boldsymbol{A},\boldsymbol{B}]$ was the internal product of vectors $\boldsymbol{A}$ and $\boldsymbol{B}$. The coordinates of a cell with an $ID=i$ at $time=t$ were represented as vector $\boldsymbol{r}(i,t)$. $|\boldsymbol{A}|$ stood for the absolute value of vector $\boldsymbol{A}$; thus, $|\boldsymbol{A}|=sqrt(dot[\boldsymbol{A},\boldsymbol{A}])$, where $sqrt(\boldsymbol{a})$ was the square root of $\boldsymbol{a}$. The coordinates were plotted against time.

The point at which a cell was overtaken was visually determined as when the centroid of the pre-existing tip cell fell behind that of the cell coming from behind for at least two frames. For tip cell parameters, 'elongation drive' (net elongation of a branch)/(number of tip cells during the total observed time) and 'tip duration' (overall time)/(number of tip cells during the total observed time) were introduced. For parameters at stalks and junctions, the 'coordination' index was set. The angle $[\theta(i,t)]$ between the direction of elongation or the bisector (elongation direction, $\boldsymbol{D}$) and the moving direction of a cell [velocity vector, $\boldsymbol{v}(i,t)$] was calculated and plotted against time. $\boldsymbol{D}$ was set so as to face the direction of net cell flow, parallel to the axis of the distal stalk, or the bisector of distal stalks if there were two outflows, at junctions. The angle was calculated by the equation, $\theta=Arccos(dot[\boldsymbol{D},\boldsymbol{v}]/|\boldsymbol{D}||\boldsymbol{v}|)$, where θ ranges from 0 to π and $\boldsymbol{v}=\boldsymbol{v}(i,t)=\boldsymbol{r}(i,t+15)-\boldsymbol{r}(i,t)$. Thus, in coordinated junctions, θs were expected to be narrowly distributed around the mean. Quantification was performed by pooling the time series and taking the standard deviation (Std) for anterograde ($\theta<\pi/2$) and retrograde ($\theta>\pi/2$) separately. The 'orientation' index was defined as (net displacement of the cell)/(total length of the track of a cell). Net displacement of a cell $[\boldsymbol{R}(i)]$ was calculated by $\boldsymbol{R}(i)=|\boldsymbol{r}(i,end)-\boldsymbol{r}(i,start)|$, where '*start*' and '*end*' referred to the time points at which the cell enters ('*start*') and moves out of ('*end*') the analyzed area, and the total

length of the track of a cell [$L(i)$] was calculated by $L(i)=\Sigma|v(i,t)|$, where sigma (Σ) was the summation for time (t=*start* to t=*end*). A value near 1 means the cell has moved straight and with no change in direction in the analyzed area. Percentages of ECs moving forwards (anterograde, $\theta<\pi/2$), backwards (retrograde, $\theta>\pi/2$) or remaining (still, $v=0$) were also calculated as the ratio to the total number of cells observed in a particular stalk area throughout the period from $t=0$ to t=*end* ('Directional motility'). ECs that moved fewer than 0.5 pixels were counted as stopped. Finally, mean absolute velocity ($<v(i)>$) at a specific area of analysis was calculated as $<v(i)>=\Sigma|v(i,t)|/\Delta t$, where Δt stood for the time interval between the start and the end.

Whole-mount staining and imaging

For murine aortic assays, whole-mount staining was performed as described previously (Yamashita et al., 2000). If needed, nuclei were counterstained with TOPRO3 (Invitrogen). For live cell imaging, SYTO-dye-stained cells were immunostained with fluorescent-conjugated anti-CD31- and PDGFRβ-Abs for 30 minutes prior to imaging. In the murine retina, whole-mount immunostaining was performed as previously described (Uemura et al., 2002). Fluorescent signals were visualized with a computer-assisted confocal microscope (Nikon D-ECLIPSE C1). Photomicrographs were obtained at 1-10 μm intervals as necessary and reconstituted using EZ-C1 software (Nikon). Signals were also visualized by an enzymatic reaction with 3,3′-diaminobenzidine (Dojin) chromogen, and photographs were obtained with a phase-contrast microscope (Nikon TE300, Tokyo, Japan).

Proliferation analysis

Mitotic events were detected on movies (see Fig. S2A in the supplementary material). The percentage was calculated by dividing the number of ECs undergoing mitosis at specified places by the total number of ECs appearing in an observed movie. Mean observed time per cell was also calculated. In addition, angiogenic sprouts were immunostained with PH3, a marker of mitosis (Hendzel et al., 1997; Dai et al., 2005), at day 7. The number of $PH3^+$ ECs was counted in randomly selected areas (including the sprout from the bottom to the tip), and the rate of $PH3^+$ ECs to total ECs per ring was calculated. Furthermore, observed areas were divided into two specified areas ('distal 400', 400 μm area proximal to the tip; 'proximal', the area more proximal than the 'distal 400'). Similar analyses were performed for murine retinal angiogenesis.

Morphology analysis

Z-stack images of $CD31^+$ endothelial sprouts were obtained using a confocal microscope as described above. After optimization on Photoshop, endothelial sheet-forming areas and parts of the explanted ring were manually eliminated. The total length of angiogenic sprouts was then measured on the converted binary images using the NeuronJ plug-in for ImageJ ('total length'). The total number of branching points was manually counted ('total branch points') and the 'relative branch point' was defined as ('total branch points')/('total length'). The 'mean width' was calculated by dividing total area of the sprouts by 'total length'.

Flow cytometry

After the explanted rings had been manually extracted from type I collagen gels, the gels were incubated in medium-199 containing 1 mg/ml collagenase (Sigma) at 37°C for 30 minutes, followed by incubation with 0.05% trypsin-EDTA (Sigma). The cells were immunostained with an anti-CD31-Ab conjugated with PE on ice. Analyses were performed on a FACS VantageSE flow-cytometer (BD Biosciences), and data were analyzed with CellQuest software (BD Biosciences). In the assay, nonviable cells stained with propidium iodide (Sigma) were excluded by electronic gating.

RT-PCR

Cells were harvested as described above. Extracted total RNA was reverse-transcribed using a conventional method. For semi-quantitative RT-PCR, the resultant cDNAs were amplified with *Taq* polymerase (Takara) in a thermocycler. The primer pairs used were as follows: for murine Hes-1, 5′-TCATGGAGAAGAGGCGAAGG/GTATTTCCCCAACACGCTCG-3′; for murine Hey2, 5′- CCGAGAGTGCTTGACAGAAGTG/TGTGGGGA-GATGGTGGAAA-3′; for murine CD31, 5′-AGGACAGACCCTTCCA-CCAA/AATGACAACCACCGCAATGA-3′; and for murine GAPDH, 5′-GGTGTGAACCACGAGAAATAT/AGATCCACGACGGACACATT-3′. Thermal cycling was performed for 18-30 cycles to maintain PCR conditions within the linear range of amplification before reaching saturation. Each cycle consisted of 30 seconds of denaturation at 94°C, 30 seconds of annealing at 58°C and 1 minute of extension at 70°C.

Statistical analysis

All data were compared between groups using the Mann-Whitney test and Kruskal-Wallis test accompanied by multi-comparison analysis where necessary. Pearson correlations were used to evaluate the relations between vessel elongation and other parameters. The relationships between vessel elongation and other parameters were studied using a linear regression analysis, which was performed separately for models involving single or multiple independent variables. The variance inflation factor was also estimated for all independent parameters in order to evaluate co-linearity. $P<0.05$ was considered significant. Data in bar graphs were represented as means±s.e.m.

RESULTS

Fluorescent imaging of ECs during in vitro angiogenesis

To characterize the behavior of vascular ECs during angiogenic morphogenesis, we visualized the dynamics of cell movement during in vitro angiogenic processes in a murine aortic ring assay (Blacher et al., 2001), using time-lapse microscopy. In this assay, various modules of the angiogenic processes such as endothelial sheet formation, sprouting, circumferential growth, branching and the resultant formation of a characteristic dendritic architecture were observed under VEGF stimulation (Fig. 1A). The sprouts of $CD31^+$ ECs were covered with $NG2^+$, $PDGFR\beta^+$ MCs (Ozerdem et al., 2001; Armulik et al., 2005), and also characterized by endothelin receptor type A (*Ednra*)-EGFP knock-in gene expression (Asai et al., 2010) (Fig. 1B-D).

To identify and track individual ECs in the multicellular structure, the nuclei of living cells were labeled with a cell-permeable fluorescent SYTO dye, by which we succeeded in selectively labeling EC during angiogenic morphogenesis (Fig. 1E-G; see Fig. S1 in the supplementary material; see also Movies 1 and 2 in the supplementary material). Although nuclear staining was not specific for ECs, we found that ECs could be distinguished from MCs covering endothelial sprouts by their signal intensity: whereas ECs showed intense staining with SYTO dyes, morphologically distinguishable or $Ednra\text{-}EGFP^+$ MCs were minimally stained (Fig. 1F; see Fig. S1C and Movie 2 in the supplementary material). In addition, this was supported by the results of live cell staining and imaging, which demonstrated that cells intensely stained with SYTO dyes were positive for CD31, whereas faintly stained cells were negative for CD31 or positive for PDGFRβ (Fig. 1G; see Fig. S1A,B in the supplementary material). The difference in SYTO dye stainability was further confirmed by flow-cytometric analysis (see Fig. S1D in the supplementary material). Thus, differences in nuclear staining as well as in morphology were used to visually distinguishing ECs from MCs.

Time-lapse live imaging reveals complexity of EC behavior during in vitro angiogenesis

In the aortic ring assay, elongation and bifurcation of an existing branch were evident. However, cellular behaviors underlying these events were far more complex and heterogeneous than expected (Fig. 2A; see Movie 1 in the supplementary material).

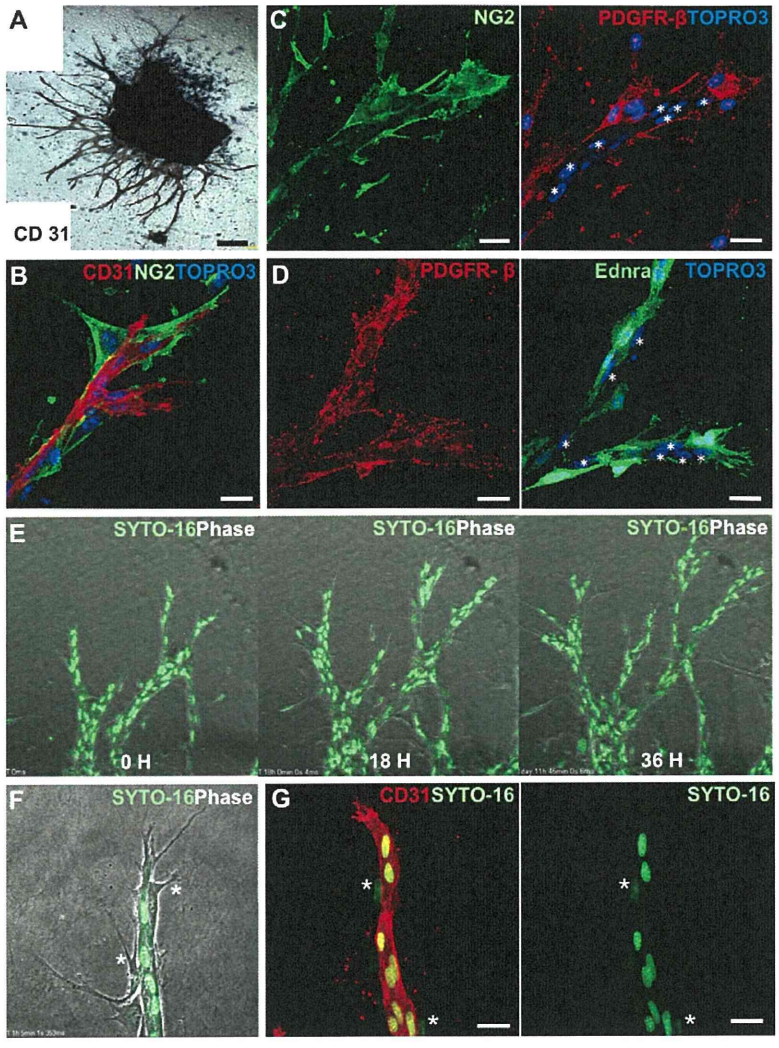

Fig. 1. Establishment of EC-tracking system in murine aortic ring assay. (**A**) CD31$^+$ EC sprouts protruding from an aortic ring explant. (**B-D**) CD31$^+$ EC sprouts are covered with MCs positive for NG2 (B), PDGFRβ (C) and Ednra-EGFP (D). Asterisks indicate nuclei of ECs. (**E**,**F**) Merged images of confocal and phase-contrast views. Nuclei were stained with SYTO dye. (E) Time-lapse images (see also Movie 1 in the supplementary material). (F) Nuclei in MCs (asterisk) were only faintly stained by SYTO dyes when compared with those in ECs. (**G**) Immunostaining confirmed that strongly SYTO dye-stained cells were CD31$^+$ ECs. Asterisks indicate CD31$^-$ MCs. Scale bars: 250 μm in A; 25 μm in B-D,G.

Individual ECs moved forwards and backwards along the path of the elongation in stalks and junctions, changing their velocity. At the tip region, fast cells overtaking other ECs become the new tip, indicating replacement of tip cells ('overtaking of the tip cell'). As a result, relative positional relationship of ECs was dynamically changed ('cell-mixing'). This 'cell-mixing' phenomenon was clearly shown by labeling cells segmentally with different colors (Fig. 2A; see Movie 1 in the supplementary material). Although the elongating process was dynamic, the frequency of cell division was very low at around 5% of total ECs in the observed time (mean observed time per cell was 22.4 hours), even in the presence of VEGF (see Table S1 in the supplementary material). Consistently, we observed that the number of PH3$^+$ ECs was quite low (0.8% of total observed ECs), with lower frequency in the proximal region (see Fig. S2B,C in the supplementary material). Observations were similar for murine retinal angiogenesis at P1 and P3 (see Fig. S2B,C in the supplementary material), also consistent with a previous report (del Toro et al., 2010). These results suggest that elongation and branching in the observed area are attributable mainly to EC migration rather than to proliferation.

Dynamics of cell movement during branch elongation

To further elucidate cell behavior in an elongating branch, we developed a trajectory analysis, which enabled us to evaluate visually and quantitatively single- and multi-cellular movements, as well as to compare the dynamics of cell movement between branches elongating in different directions (Fig. 2B; see Fig. S3 in the supplementary material). Trajectory analysis revealed that branch elongation was a repeated event in which an EC at the stalk overtook the tip cell to become the new tip (Fig. 2B, part a). The new tip cell became less motile after this overtaking (arrow), followed by being overtaken by another cell (arrowhead). Thus, branch elongation appeared to be promoted by repetitive overtaking (a dark-blue trajectory in Fig. 2B, part a). In some cases, a tip cell was overtaken by another EC (arrow) and then retreated to become a tip cell again (arrowhead) (purple trajectory in Fig. 2B, part b). Furthermore, overtaking (arrow) by a fast-moving EC from far behind (fast EC, a pink trajectory in Fig. 2B, part c) seemed to contribute to effective branch elongation. In a poorly elongating branch, overtaking by a fast EC was rare (arrowhead in Fig. 2B, part c). However, overtaking by a fast EC alone was not sufficient

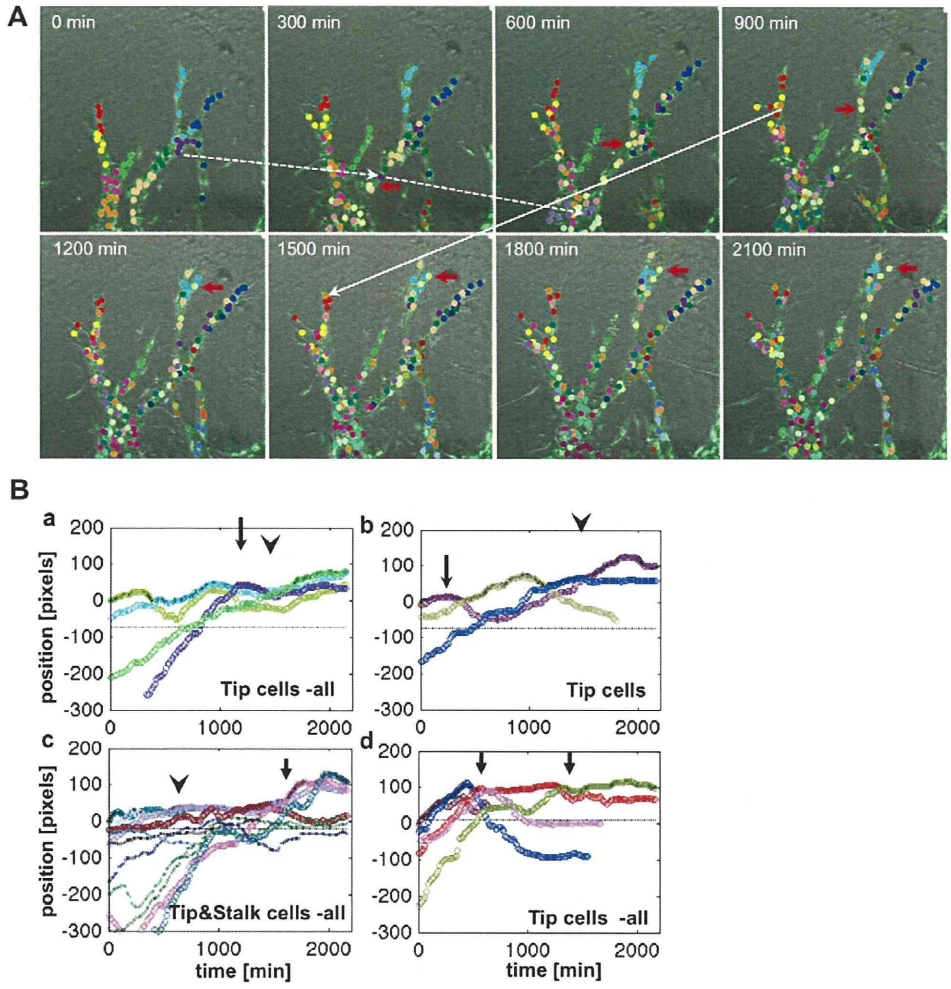

Fig. 2. Time-lapse live imaging and computational analysis reveals complexity of EC behaviors during in vitro angiogenesis. (**A**) SYTO dye-staining and time-lapse imaging were performed in the aortic ring assay. *Z*-stack confocal images were overlaid on the phase-contrast images. Nuclei were tracked using MTrackJ and the centroids of these nuclei are pseudocolored clusterwise. Initial clusterwise labeling becomes increasingly obscure over time ('cell-mixing'). Yet ECs are seen to move faster than others and become the new tip (white and red arrows). Some other ECs are seen to move in the direction opposite elongation (broken arrow) (see also Movie 1 in the supplementary material). (**B**) Trajectory analysis. Representative patterns of EC movements during branch elongation are shown. Cells that became tip cells at some point are represented by thick lines; individual cells are presented in different colors (see also Fig. S3 in the supplementary material). (a) Repeated overtaking of the tip cell during branch elongation. (b) Repetitive overtaking of the tip cell by an EC. (c,d) Overtaking by a fast-moving EC resulting in effective branch elongation (c) or not (d).

for elongation because some branches with overtaking by a fast EC did not show effective elongation (arrows in Fig. 2B, part d), suggesting that other conditions in which overtaking by a fast EC leads to effective elongation are also necessary.

Mosaic analysis confirms 'cell-mixing' phenomenon during in vitro angiogenesis

To confirm whether the identified phenomena such as 'cell-mixing' based on nuclear tracking occur on a whole-cell basis, we performed a mosaic analysis by visualizing the cytoplasm with EGFP. In this analysis, ECs could be identified by differences in the intensity of SYTO dye staining and, in some cases, staining for BS-1 lectin (Fig. 3). Mosaic analysis revealed that high EGFP-labeled EC (red arrows in Fig. 3A) appeared to 'slip' forward on the surface of a tip cell, overtaking and then being replaced by a follower EC without the EGFP signal (yellow arrows), which confirmed overtaking of the tip cell at a cellular level (see Movie 3 in the supplementary material). Mosaic analysis further showed that highly motile ECs displayed unidirectional forward-rear cell polarity, depending on the direction of movement, whereas minimally motile ECs were spindle-shaped without cell polarity (Fig. 3A-D; see Movies 3 and 4 in the supplementary material), and that the polarity of individual ECs was dynamically changed in conjunction with the motility (Fig. 3E; see Movie 5 in the supplementary material). These results provide a cellular basis for the phenomenon of angiogenic sprouting with 'cell-mixing'.

Identification of 'cell-mixing' phenomenon during murine retinal angiogenesis in vivo

Next, we verified whether the 'cell-mixing' phenomenon occurs in vivo. We labeled ECs by intravascular injection of a BS-1 lectin at postnatal day 1.0 and tracked them during mouse retinal

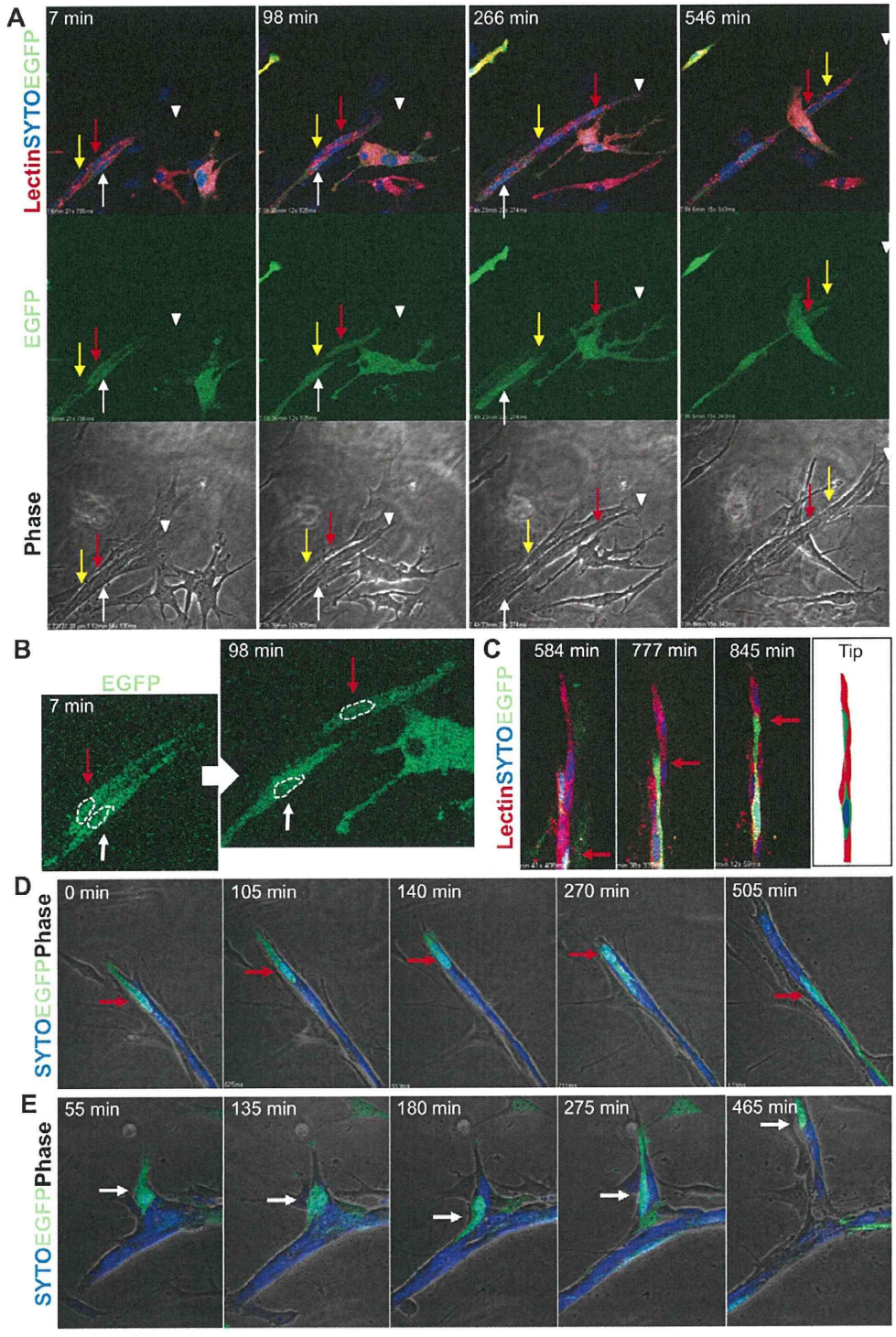

Fig. 3. Mosaic analysis reveals 'cell-mixing' phenomenon on whole-cell basis. In the aortic ring assay, in which cells were infected with a low titer of adenovirus carrying EGFP, time-lapse imaging was performed. ECs were identified by stainability with SYTO dye and/or BS-1 lectin. (**A**) Representative time-lapse images showing 'overtaking of the tip cell' (red and yellow arrows). White arrowheads indicate the tip of the endothelial sprout. White arrows indicate minimally motile ECs. (**B**) Higher magnification images of A, showing highly motile (red arrow) and minimally motile (white arrows) ECs. Broken circles indicate nuclei (see Movie 3 in the supplementary material). (**C**) Another example of a highly motile EC (red arrow). (**D**) Cell polarity changed dynamically depending on the direction of movement (red arrow) (see Movie 4 in the supplementary material). (**E**) An EC (white arrow), which lost cell polarity just before being overtaken by a follower (135 minutes), generated cell polarity again at 275 minutes and again started moving to the tip (see Movie 5 in the supplementary material).

angiogenesis (Fig. 4A). At this stage, sprouting angiogenesis takes place on the retinal surface (Fig. 4B), and tip and distal stalk cells do not form a lumen (Gerhardt et al., 2003). Consistent with previous findings, the proximal (lumen-forming) regions of $CD31^+$ endothelial sprouts were uniformly and reproducibly labeled by lectin shortly after its injection, whereas the distal regions (including the tip) were not (Fig. 4C). As expected, 6 hours after the injection, lectin-positive and -negative cells were colocalized at the distal regions in a mixed pattern. Typically, a $CD31^+$ EC at the tip and some follower ECs were lectin positive in the distal regions (Fig. 4C; see Fig. S4A in the supplementary material), indicating that the ECs around the tip came from the proximal regions forming the lumen. Similar mosaic patterns were also observed at the distal and proximal positions of sprouts 12 hours after the lectin injection (see Fig. S4B in the supplementary material). Collectively, these results strongly suggest that the 'cell-mixing' phenomenon occurs during in vivo retinal angiogenesis.

Quantification of EC behaviors driving angiogenic morphogenesis

In order to unravel the cell-based mechanism that drive angiogenic morphogenesis and dissect the underlying molecular networks, we first set out parameters to quantify different angiogenic modules. VEGF also promoted angiogenesis in our setting (Fig. 5A; see Movie 6 in the supplementary material). One of the pro-angiogenic effects of VEGF is to elongate vessel branch, characterized herein by an increase in the index 'vessel elongation' (Fig. 5C), owing to the increased number of ECs in the branch (Fig. 5D). The tip of an elongating branch overtaking ECs was identified (Fig. 5B). Because overtaking of tip cells occurred regardless of the presence or absence of VEGF, we established 'elongation drive' (displacement per tip cell) and 'tip duration' (the time spent as a tip cell) parameters to quantify events at the tip further (Fig. 5B). Interestingly, VEGF-induced vessel elongation was closely associated only with greater elongation drive (Fig. 5C). Overtaking of tip cells occurred similarly at interval ranging from ~350 to ~900 minutes, whether or not VEGF was present. These results indicate that VEGF positively affects tip cell behaviors following overtaking without changing the frequency of overtaking.

We also set the following parameters to evaluate the complex cell movements at junctions and stalks: mean migratory velocity, coordination (whether or not ECs moved in the same direction (coordinated)), orientation (whether or not a single cell moved straightly), and directional motility (whether or not ECs migrated toward the direction of branch elongation) (Fig. 5E). In the

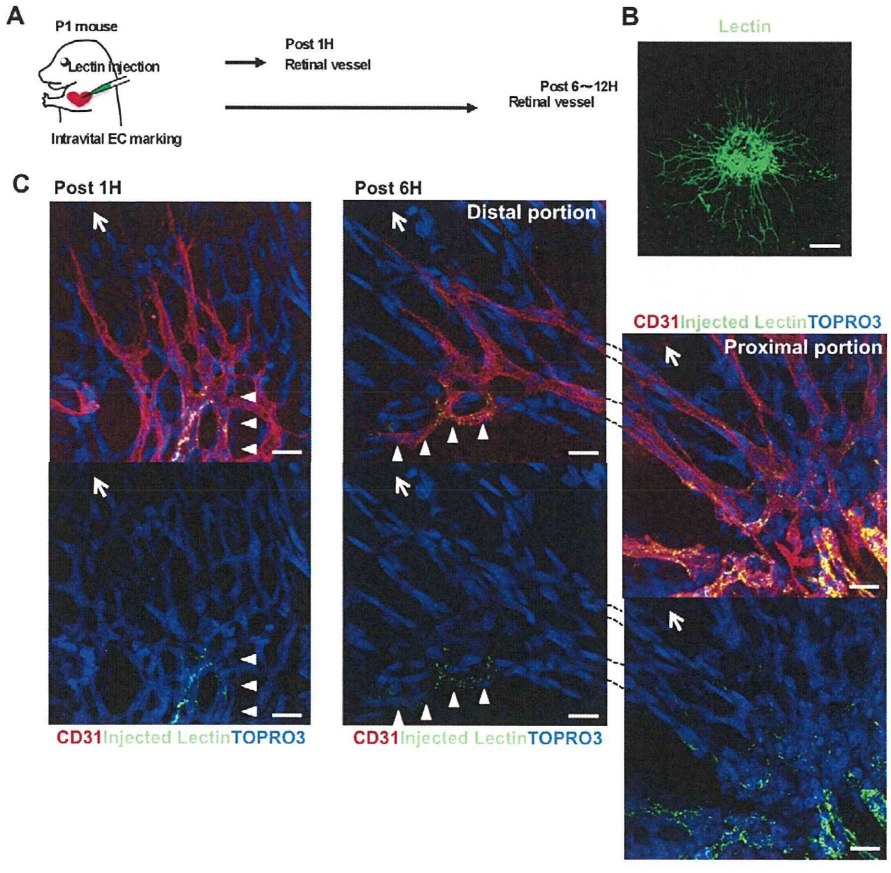

Fig. 4. Identification of 'cell-mixing' phenomenon during murine retinal angiogenesis in vivo. (**A**) BS-1 lectin was injected into the cardiac chamber at postnatal day 1 (P1) to label ECs transvacularly. Labeled ECs were observed in retinal angiogenesis 6 hours after the injection. (**B**) Whole-mount staining of the retinal vasculature with BS-1 lectin at P1. (**C**) *Z*-stack confocal images. Nuclei were stained with TOPRO3. The proximal regions of $CD31^+$ endothelial sprouts were uniformly labeled by injected lectin (arrowheads), whereas the distal regions (including the tip) were not at 1 hour after the injection. Six hours after the injection, lectin-labeled ECs (arrowheads) were also observed in some distal regions of the sprouts. Arrows show the direction of vessel elongation. Scale bars: 100 μm in B; 25 μm in C. See Fig. S4 in the supplementary material.

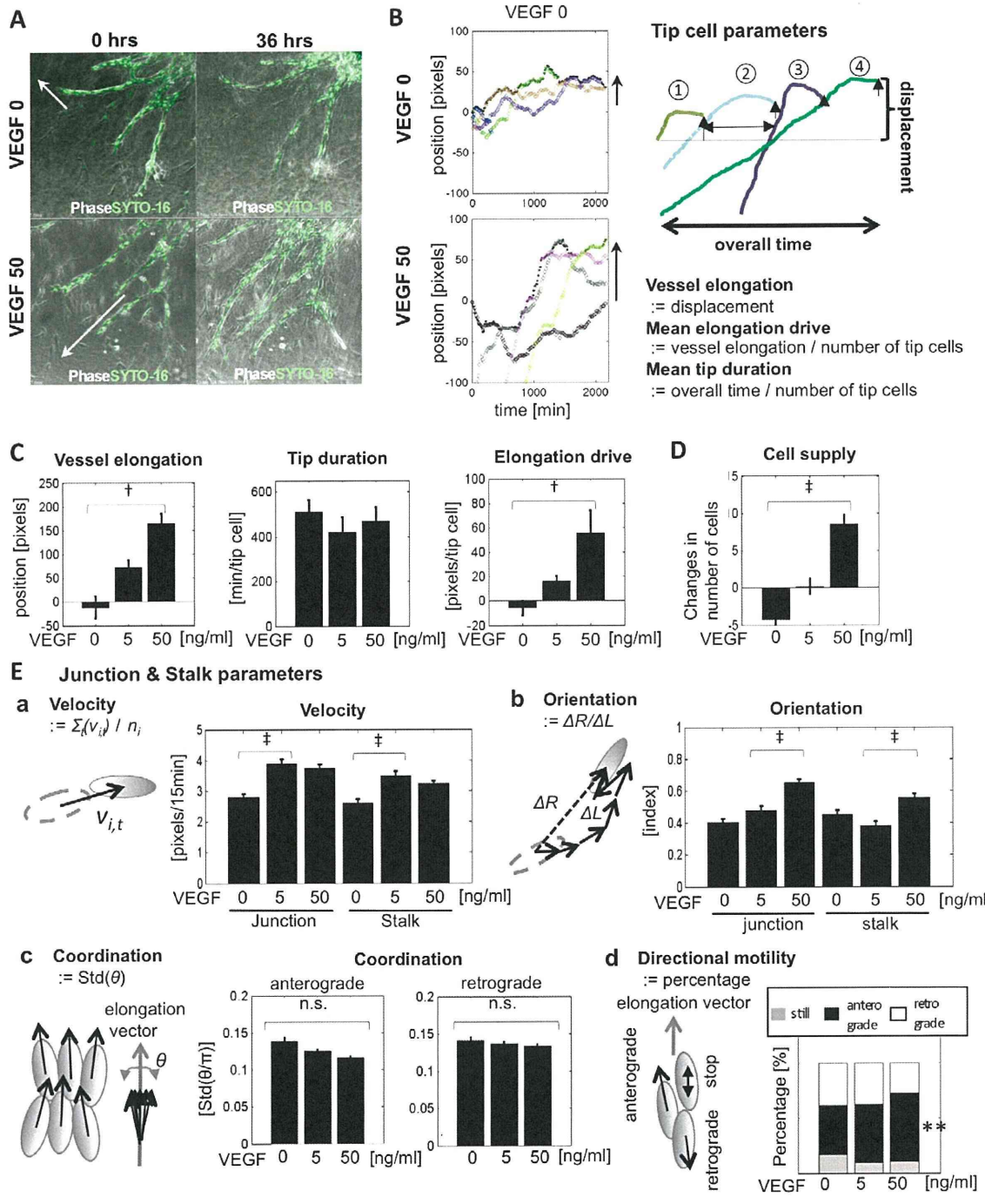

Fig. 5. Quantification of EC behaviors driving VEGF-induced angiogenic morphogenesis. (**A**) Time-lapse imaging in the murine aortic ring assay with or without VEGF. Arrows show the elongation vectors of selected branches (see also Movie 6 in the supplementary material). (**B**,**C**) Trajectory analysis (B, left panel) and parameters related to tip cells (B, right panel; C). (**D**) Cell supply (defined as changes in the number of cells in a branch). (**E**) Parameters at junctions and stalks. (a) EC velocity. (b) Orientation. (c) Coordination. (d) Directional motility (** significantly different from VEGF 0 ng/ml). Data are presented as mean±s.e.m. $^{**}P<0.01$, $^{\dagger}P<0.001$, $^{\ddagger}P<0.0001$.

presence of VEGF, ECs exhibited higher velocity and orientation at junctions and stalks (Fig. 5E-a,E-b). Coordination tended to be improved (P=0.051, for VEGF 0 ng/ml versus 50 ng/ml, Fig. 5E-c). At stalks, there was a higher proportion of ECs showing anterograde movement (Fig. 5E-d). Taken together, these data suggest that VEGF enhanced directed migration of ECs in the elongating direction at junctions and stalks. Parameters presented here are summarized in Fig. S6A in the supplementary material.

Dll4-Notch signaling pathway in collective EC movement driving angiogenic morphogenesis

To further define the molecular machinery involved in collective EC movements during angiogenesis, we interrupted Dll4-Notch signaling, which is crucial for tip cell regulation and proper angiogenesis (Hellstrom et al., 2007; Suchting et al., 2007). Consistent with previous findings (Claxton and Fruttiger, 2004; Hellstrom et al., 2007; Hofmann and Luisa Iruela-Arispe, 2007), Dll4 was expressed in ECs at the tip and, to a lesser extent, at stalks of angiogenic sprouts, but never in MCs (Fig. 6A). Dll4-Notch signaling was inhibited using a neutralizing Dll4-Ab (Yamanda et al., 2009). The inhibitory effect was confirmed by downregulation of *Hey2*, a Notch downstream target gene (Fig. 6B). In the aortic ring assay, Dll4-Ab treatment resulted in morphological changes with increased vessel branching and total sprout length (see Fig. S5A in the supplementary material), resembling the vascular phenotype in the retina and tumors of Dll4-mutant mice (Noguera-Troise et al., 2006; Hellstrom et al., 2007; Suchting et al., 2007).

In parametrical analysis, Dll4-Ab treatment enhanced vessel elongation with a concomitant increase in the EC number in each branch in the presence of VEGF (Fig. 6D,E), but did not affect the pattern of tip cell overtaking (Fig. 6C). The increase in vessel elongation was due to increased mean elongation drive without changes in mean tip duration (Fig. 6D). Dll4-Ab treatment also affected stalk cell behavior: mean EC velocity was increased at junctions and stalks, and the 'still' cell population was decreased, whereas other parameters were not changed by Dll4-Ab treatment (Fig. 6F). Increases in vessel elongation and mean velocity of ECs were also obvious in moving images (see Movie 7 in the supplementary material).

Dll4-Notch signaling was also inhibited by treatment with DAPT (Hellstrom et al., 2007; Suchting et al., 2007). This inhibitory effect was confirmed by downregulation of *Hes1*, another Notch downstream target gene (Fig. 6B). In addition, DAPT treatment eventually reduced Dll4 protein in ECs, suggesting inhibition Notch signaling was occurring (Jakobsson et al., 2010) (Fig. 6A). DAPT treatment enhanced branching formation in the same way as Dll4-Ab treatment, although there was no change in the total length of angiogenic sprouts, and sprouts were also wider, reflecting in vivo morphological changes induced by DAPT (see Fig. S5B in the supplementary material) (Hellstrom et al., 2007; Suchting et al., 2007). In parametrical analysis, unexpectedly, DAPT treatment recapitulated only the two Dll4-Ab-induced parametric changes in mean EC velocity and directional motility profiles (Fig. 6C-F; see Movie 8 in the supplementary material). Comparisons of parametric changes between Dll4-Ab and DAPT treatments are summarized in Table 1. The parametric similarities clearly suggest that the Dll4-Notch signaling pathway negatively regulates mean velocity in collective EC movements at stalks and junctions.

Role of EC-MC interaction in collective EC movement driving angiogenic morphogenesis

DAPT can inhibit not only Notch signaling (Hellstrom et al., 2007; Suchting et al., 2007) but also other γ-secretase-dependent pathways (Boulton et al., 2008), some of which are involved in interplays between EC and MC (Gaengel et al., 2009; Liu et al., 2009). Indeed, the number of $NG2^+$, $Ednra\text{-}EGFP^+$ MCs covering endothelial sprouts was decreased (Fig. 7A). To test whether the differences between the effects of Dll4-Ab and DAPT are attributable to Dll4-independent EC-MC interactions, the cells were treated with PDGFRβ-Ab, which interrupts proper covering of endothelial sprouts by MCs and the resulting EC-MC interactions (Uemura et al., 2002; Jin et al., 2008; Liu et al., 2009). As expected, the association between ECs and $NG2^+$, $Ednra\text{-}EGFP^+$ MCs was diminished by PDGFRβ-Ab, while endothelial sprouting was evident (Fig. 7A). Interestingly, moving images showed that PDGFRβ-Ab treatment apparently increased ECs moving in the direction opposite branch elongation, resulting in retarded branch elongation (see Movie 9 in the supplementary material). Accordingly, parametric analysis revealed that both mean tip duration and elongation drive were decreased by PDGFRβ-Ab treatment with a preserved pattern of tip cell overtaking (Fig. 7B,C). In addition, PDGFRβ-Ab treatment increased retrograde directional motility and decreased the orientation index without changes in velocity or coordination (Fig. 7D), indicating disturbed directional movement. These results recapitulated a portion of the DAPT-induced parametric changes, which had not been observed with Dll4-Ab (Table 1). The similarities in parametrical changes between PDGFRβ-Ab and DAPT suggest that MCs may affect behaviors of tip cells and directed migration at stalks with collective EC movement in a γ-secretase-dependent manner. However, the parametrical changes in response to DAPT treatment might also be due to alterations of EC-EC interplay via γ-secretase-dependent pathways other than the Dll4-Notch pathway.

Molecular and cellular mechanisms driving vessel elongation

Relationships between parametrical changes and the angiogenic factors studied herein are summarized in Fig. 7E. To identify which compartment of the collective EC movement most efficiently contributes to branch elongation, we analyzed correlations between the vessel elongation index and other parameters. Preliminary analyses highlighted elongation drive and velocity at junctions as possible positive explanatory variables and retrograde directional motility as a possible negative explanatory variable (see Fig. S6B,C in the supplementary material). Then, we tested whether the above three parameters can explain vessel elongation by using a multi-regression model. The results suggested elongation drive, velocity at junctions and retrograde directional motility to be significant determinants of vessel elongation in the present setting (Fig. 7F).

Therefore, the parametrical analyses collectively suggested a model possibly explaining the molecular and cellular mechanisms underlying branch elongation (Fig. 7G); VEGF induces vessel elongation by enhancing the elongation drive, velocity and percentage of anterograde directional motility, with elongation drive and velocity being counteracted by Dll4-Notch signaling. MCs may act on ECs to promote elongation drive at the tip and the directional motility that drives branch elongation.

DISCUSSION

Herein, we established a system for spatiotemporally assessing collective EC movements involved in in vitro angiogenesis using live-cell imaging with time-lapse microscopy and computational analysis. This system revealed complex and heterogeneous EC behaviors during angiogenesis: individual ECs migrate forwards and backwards at different velocities, changing their relative positions within the branch network ('cell-mixing'), even at the tip ('overtaking of the tip cell'). Based on an EC-tracking analysis of murine retina, the 'cell-mixing' phenomenon also very likely to occur during in vivo angiogenesis. Parametrical and statistical analyses further demonstrated the molecular and cellular mechanisms underlying collective EC movement. EC-EC interplay via Dll4-Notch signaling counteracts VEGF-induced tip cell elongation and

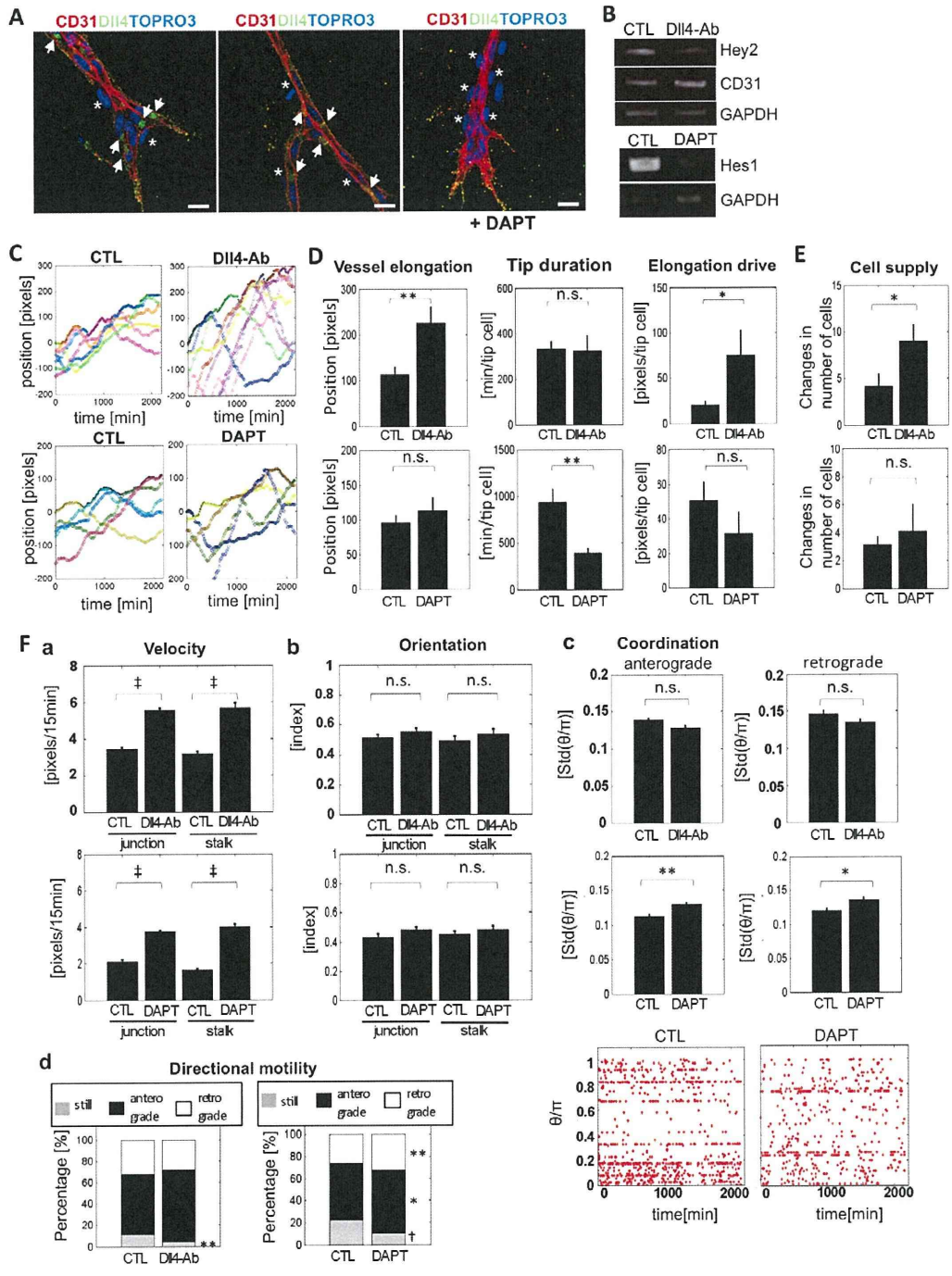

Fig. 6. Dll4-Notch signaling between ECs affects collective EC movements driving vessel elongation. (**A**) Whole-mount double staining of aortic ring assays with or without DAPT treatment. Nuclei were stained with TOPRO3. Dll4 was detected as a lump (arrows) in CD31$^+$ ECs not only at the tip (left panel) but also at the stalk (middle panel), but never in MCs (asterisks). Levels of Dll4 protein in ECs were reduced by DAPT treatment. Scale bars: 25 μm. (**B**) RT-PCR revealed Hey2 and Hes1 expression to be downregulated in cells treated with Dll4-Ab or DAPT, respectively. (**C**) Representative trajectories of tip cells. (**D**) Parameters related to tip cells. (**E**) Cell supply. (**F**) Parameters at junctions and stalks. (a) EC velocity. (b) Orientation. (c) Coordination. Scattered plots show representative of coordination analysis data. (d) Directional motility. See Movies 7 and 8 in the supplementary material. Data are presented as mean±s.e.m. *P<0.05, **P<0.01, $^{\dagger}P$<0.001, $^{\ddagger}P$<0.0001. CTL indicates control.

directed migration. In addition, EC-MC interplay might positively regulate the EC elongation and directional motility, implying a novel role of MCs in the early stage of angiogenesis.

The 'cell-mixing' phenomenon during angiogenesis was unexpected because angiogenic elongation was assumed to be a quasi-static phenomenon in which tip cells with filopodia lead the

Table 1. Effects of Dll4-Ab, DAPT and PDGFRβ-Ab treatments for analyzed parameters

Structure	Parameter	Dll4-Ab	DAPT	PDGFRβ-Ab
Tip	Vessel elongation	↑	→	↓ or →
	Tip duration	→	↓	↓
	Elongation drive	↑	↓ or →	↓
Junction and stalk	Velocity	↑	↑	→
	Orientation	→	→	↓ or →
	Coordination	→	↓	→
	Anterograde motility	→	↑	→
	Retrograde motility	→	↑	↑
	No motility	↓	↓	→

Arrows ↑, ↓ and → indicate significant increase, significant decrease and no change in each parameter, respectively.

way as pioneer cells and a chain of followers serve as stalk cells, which are connected to each other by cell-cell junctions, elongating the sprout via proliferation (Holderfield and Hughes, 2008; De Smet et al., 2009). The present findings indicate that the two distinct cellular phenotypes, tip and stalk, are interchangeable and branches elongate via a mixture of migratory ECs supplied from upstream vascular beds. Accordingly, gene expression patterns characteristic of tip and stalk cells (Phng and Gerhardt, 2009) may depend on positional context within an elongating branch. As for the phenomenon of tip cell overtaking, Jakobsson et al. reported similar findings in both in vitro and in vivo settings (Jakobsson et al., 2010) while we were preparing this manuscript. Taken together with theirs, our findings strongly suggest that cellular behaviors during angiogenesis may be more variable and complex than previously thought.

What is the biological significance of overtaking of tip cell? After one overtaking event, the new tip cell slows and elongation stops after a while, and the cell is then overtaken by the next one, leading us to speculate that the major role of a tip cell may be not only to elongate in itself but also to create a milieu suitable for the next cell. ECs express various matrix metalloproteinases which degrade the surrounding extracellular matrix (ECM) and thereby create space for invasion (van Hinsbergh and Koolwijk, 2008). Furthermore, a recent report (del Toro et al., 2010) on murine retinal neovessels showed that genes involved in ECM remodeling, such as urokinase-plasminogen-activated receptor and nidogen 2, were enriched in the tip cells. Indeed, a tip cell seems to serve as a 'rail' for the following new cell, and this machinery may also explain the 'cell-mixing' phenomenon observed at stalks and junctions.

Interestingly, some ECs migrated backwards when the branch was elongating forwards. Previous reports have shown that gradients of local VEGF appear to provide tip cell migration directionality in the retina (Stone et al., 1995; Provis et al., 1997; Gerhardt et al., 2003). Because the local VEGF gradient would presumably be canceled with addition of a large amount of VEGF to the culture medium in our experimental system, retrograde EC movement may merely reflect a loss of the VEGF gradient. However, administration of VEGF resulted in increased anterograde EC migration at stalks without any gradient. This suggests that there is an additional force driving movement towards the tip. In fact, the present parametrical analysis showed that inhibition of both Dll4-Notch signaling and EC-MC interaction also affected the directionality of EC migration. Thus, mechanisms determining directionality are complex, and VEGF may function to enhance directional movement independently of its regional gradient. At the moment, whether the retrograde EC migration occurs in in vivo angiogenesis is unknown. Even though our observations may not represent a physiological phenomenon, they may provide clues to the mechanism responsible for directionality.

The present results provide clues as to how the spatiotemporal regulation of molecular interactions collectively affect EC behaviors, resulting in branch elongation. The VEGFR-Dll4-Notch circuit is reported to be crucial for tip cell function (Hellstrom et al., 2007; Suchting et al., 2007). Similarly, in the present study, interrupting VEGF and Dll4-Notch signaling pathways affected tip cell behavior, as analyzed by the 'elongation drive' index. More recently, Jakobsson et al. demonstrated that the signal circuit contributes to tip cell selection and the resultant tip cell replacement (Jakobsson et al., 2010). In the present study, however, the frequency of tip overtaking was unchanged regardless of the absence or presence of VEGF or inhibition of Dll4-Notch signaling. Our results imply that another mechanism may drive overtaking of the tip cell. The parametric analysis results suggest γ-secretase-dependent machinery other than the Dll4-Notch pathway and/or EC-MC interplay possibly to control the frequency of tip cell overtaking.

In conjugation with tip cell navigation, migratory behaviors of ECs following the tip cell affected branch elongation as previously assumed (Schmidt et al., 2007; Perryn et al., 2008). VEGF enhanced the velocity and directionality of EC migratory behaviors, resulting in efficient branch elongation, whereas Dll4-Notch signaling exerted inhibitory actions on both. The string of inhibitory actions exerted by the Dll4-Notch pathway may be due to downregulation of VEGFR2 (Ridgway et al., 2006; Williams et al., 2006). Another possibility is that Notch activation might inhibit EC migration via an Id1-dependent mechanism, which potently contributes to angiogenesis (Itoh et al., 2004; Nishiyama et al., 2005). Considering the mosaic expression pattern of Dll4 throughout angiogenic sprouts, Dll4-Notch interactions occur widely between ECs within sprouts, and scattered activation of the Dll4-Notch signal seems to partially explain the heterogeneity of EC movements. Collectively, these results raise the possibility of a yet-to-be defined role of the Dll4-Notch signaling pathway in controlling EC movements at stalks and junctions.

The present study demonstrated that EC-MC interaction might affect collective EC movement driving branch elongation. In particular, the suppressive action on backwards EC movement was marked. MCs are widely accepted as playing a pivotal role in the process of vessel maturation and remodeling at the late stage of angiogenesis. However, the biological significance of MCs in the early stage remained largely unknown, despite MCs having identified in proximity to sprouting ECs during angiogenesis of the developing brain and retina (Bauer et al., 1992; Ozerdem and Stallcup, 2003). Therefore, this observation suggests a novel role

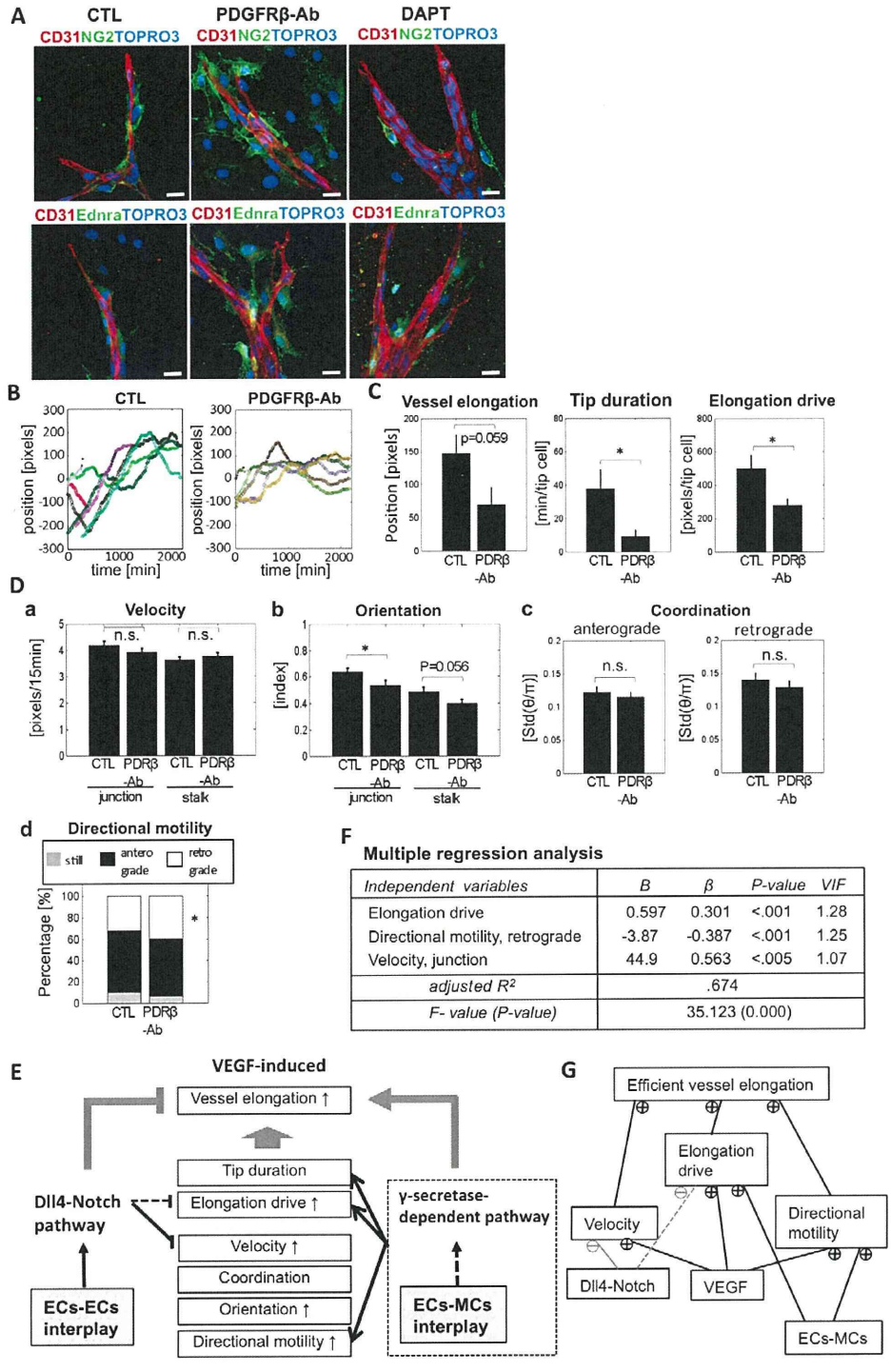

Fig. 7. Molecular and cellular mechanisms for vessel elongation by EC-EC and EC-MC interactions. Time-lapse imaging was performed in murine aortic ring assays with PDGFRβ-Ab treatment. (**A**) Whole-mount staining in the assay using the wild-type or *Ednra*^{egfp} mouse with the indicated treatment. Nuclei were stained with TOPRO3. Scale bars: 25 μm. (**B**) Representative trajectories of tip cells. (**C**) Parameters related to tip cells. (**D**) Parameters at junctions and stalks. (a) EC velocity. (b) Orientation. (c) Coordination. (d) Directional motility. PDGFRβ-Ab treatment tended to decrease vessel elongation, while clearly decreasing elongation drive and tip duration. See also Movie 9 in the supplementary material. Data are presented as mean±s.e.m. **P*<0.05. CTL and PDR-β indicate control and PDGFRβ, respectively. (**E**) The summary of parametrical changes and their underlying molecular pathways. (**F**) Multi-regression analysis. *B*, unstandardized coefficient; β, standardized coefficient; *VIF*, variance inflation factor. (**G**) A possible model explaining molecular and cellular mechanisms underlying vessel elongation. Minus marks and gray indicate inhibitory effects.

for MCs in angiogenesis. The present study further indicated that a γ-secretase-dependent pathway other than the Dll4-Notch pathway might contribute to the EC-MC interplay. γ-Secretase activates the Notch signal via cleavage of its receptor and a jagged 1 ligand is expressed in MCs (Domenga et al., 2004; Liu et al., 2009). γ-Secretase activity also regulates the dynamics of cadherins (Boulton et al., 2008), which mediate morphogenetic movements (Gumbiner, 2005; Theveneau et al., 2010). Thus, MCs may use the jagged 1-Notch pathway and/or the cadherin-mediated cell-adhesion system for the interplay with ECs, resulting in the control of collective EC movements during angiogenesis.

In conclusion, we have developed a time-lapse imaging and quantitative analysis system revealing cell-based mechanisms underlying elongation processes during in vitro angiogenesis. The physiological relevance of 'cell mixing', one of our major findings, was confirmed by analysis of in vivo retinal angiogenesis. The biological findings reported herein and the parameters that we defined can be incorporated in an agent-based model to simulate angiogenic cell behavior, which may in turn yield new insights for understanding the sprouting, elongating and branching aspects of angiogenesis. Furthermore, the methodology employed may allow the gaps among molecular, cellular and integrative bases of organic morphogenesis to be bridged.

Acknowledgements
We thank Olympus Corporation for multiple trials on FluoView FV10i, Dr Shin-ichi Nishikawa and Dr Akiyoshi Uemura for antibodies, and Dr Hideyuki Sakoda for the adenovirus. We also thank Yuko Fujisawa, Takahiro Sato, Rieko Asai and Sakura Kushiyama for excellent technical assistance. MTrackJ was developed at the Biomedical Imaging Group Rotterdam of the Erasmus MC-University Medical Center Rotterdam (The Netherlands) by Erik Meijering.

Funding
This work was supported in part by the Global COE Program (Integrative Life Science Based on the Study of Biosignaling Mechanisms) from the Ministry of Education, Culture, Sports, Science and Technology (MEXT, Japan); by grants-in-aid for scientific research from MEXT (Japan) [23111505 to K.N.]; by grants-in-aid for scientific research from the Ministry of Health, Labour and Welfare of Japan [09156294 to H.K.]; and by grants-in-aid for scientific research from Japan Society for the Promotion of Science (JSPS, Japan) [23591099 to K.N., 21390238 to H.K.].

Competing interests statement
The authors declare no competing financial interests.

Supplementary material
Supplementary material for this article is available at
http://dev.biologists.org/lookup/suppl/doi:10.1242/dev.068023/-/DC1

References
Armulik, A., Abramsson, A. and Betsholtz, C. (2005). Endothelial/pericyte interactions. *Circ. Res.* **97**, 512-523.
Asai, R., Kurihara, Y., Fujisawa, K., Sato, T., Kawamura, Y., Kokubo, H., Tonami, K., Nishiyama, K., Uchijima, Y., Miyagawa-Tomita, S. et al. (2010). Endothelin receptor type A expression defines a distinct cardiac subdomain within the heart field and is later implicated in chamber myocardium formation. *Development* **137**, 3823-3833.
Bauer, H. C., Steiner, M. and Bauer, H. (1992). Embryonic development of the CNS microvasculature in the mouse: new insights into the structural mechanisms of early angiogenesis. *EXS* **61**, 64-68.
Blacher, S., Devy, L., Burbridge, M. F., Roland, G., Tucker, G., Noel, A. and Foidart, J. M. (2001). Improved quantification of angiogenesis in the rat aortic ring assay. *Angiogenesis* **4**, 133-142.
Boulton, M. E., Cai, J. and Grant, M. B. (2008). gamma-Secretase: a multifaceted regulator of angiogenesis. *J. Cell. Mol. Med.* **12**, 781-795.
Claxton, S. and Fruttiger, M. (2004). Periodic Delta-like 4 expression in developing retinal arteries. *Gene Expr. Patterns* **5**, 123-127.
Dai, J., Sultan, S., Taylor, S. S. and Higgins, J. M. (2005). The kinase haspin is required for mitotic histone H3 Thr 3 phosphorylation and normal metaphase chromosome alignment. *Genes Dev.* **19**, 472-488.
De Smet, F., Segura, I., De Bock, K., Hohensinner, P. J. and Carmeliet, P. (2009). Mechanisms of vessel branching: filopodia on endothelial tip cells lead the way. *Arterioscler. Thromb. Vasc. Biol.* **29**, 639-649.
del Toro, R., Prahst, C., Mathivet, T., Siegfried, G., Kaminker, J. S., Larrivee, B., Breant, C., Duarte, A., Takakura, N., Fukamizu, A. et al. (2010). Identification and functional analysis of endothelial tip cell-enriched genes. *Blood* **116**, 4025-4033.
Domenga, V., Fardoux, P., Lacombe, P., Monet, M., Maciazek, J., Krebs, L. T., Klonjkowski, B., Berrou, E., Mericskay, M., Li, Z. et al. (2004). Notch3 is required for arterial identity and maturation of vascular smooth muscle cells. *Genes Dev.* **18**, 2730-2735.
Friedl, P. and Gilmour, D. (2009). Collective cell migration in morphogenesis, regeneration and cancer. *Nat. Rev. Mol. Cell Biol.* **10**, 445-457.
Gaengel, K., Genove, G., Armulik, A. and Betsholtz, C. (2009). Endothelial-mural cell signaling in vascular development and angiogenesis. *Arterioscler. Thromb. Vasc. Biol.* **29**, 630-638.
Gerhardt, H., Golding, M., Fruttiger, M., Ruhrberg, C., Lundkvist, A., Abramsson, A., Jeltsch, M., Mitchell, C., Alitalo, K., Shima, D. et al. (2003). VEGF guides angiogenic sprouting utilizing endothelial tip cell filopodia. *J. Cell Biol.* **161**, 1163-1177.
Gumbiner, B. M. (2005). Regulation of cadherin-mediated adhesion in morphogenesis. *Nat. Rev. Mol. Cell Biol.* **6**, 622-634.
Hellstrom, M., Gerhardt, H., Kalen, M., Li, X., Eriksson, U., Wolburg, H. and Betsholtz, C. (2001). Lack of pericytes leads to endothelial hyperplasia and abnormal vascular morphogenesis. *J. Cell Biol.* **153**, 543-553.
Hellstrom, M., Phng, L. K., Hofmann, J. J., Wallgard, E., Coultas, L., Lindblom, P., Alva, J., Nilsson, A. K., Karlsson, L., Gaiano, N. et al. (2007). Dll4 signalling through Notch1 regulates formation of tip cells during angiogenesis. *Nature* **445**, 776-780.
Hendzel, M. J., Wei, Y., Mancini, M. A., Van Hooser, A., Ranalli, T., Brinkley, B. R., Bazett-Jones, D. P. and Allis, C. D. (1997). Mitosis-specific phosphorylation of histone H3 initiates primarily within pericentromeric heterochromatin during G2 and spreads in an ordered fashion coincident with mitotic chromosome condensation. *Chromosoma* **106**, 348-360.
Hofmann, J. J. and Luisa Iruela-Arispe, M. (2007). Notch expression patterns in the retina: an eye on receptor-ligand distribution during angiogenesis. *Gene Expr. Patterns* **7**, 461-470.
Holderfield, M. T. and Hughes, C. C. (2008). Crosstalk between vascular endothelial growth factor, notch, and transforming growth factor-beta in vascular morphogenesis. *Circ. Res.* **102**, 637-652.
Itoh, F., Itoh, S., Goumans, M.-J., Valdimarsdottir, G., Iso, T., Dotto, G. P., Hamamori, Y., Kedes, L., Kato, M. and ten Dijke, P. (2004). Synergy and antagonism between Notch and BMP receptor signaling pathways in endothelial cells. *EMBO J.* **23**, 541-551.
Jakobsson, L., Franco, C. A., Bentley, K., Collins, R. T., Ponsioen, B., Aspalter, I. M., Rosewell, I., Busse, M., Thurston, G., Medvinsky, A. et al. (2010). Endothelial cells dynamically compete for the tip cell position during angiogenic sprouting. *Nat. Cell Biol.* **12**, 943-953.
Jin, S., Hansson, E. M., Tikka, S., Lanner, F., Sahlgren, C., Farnebo, F., Baumann, M., Kalimo, H. and Lendahl, U. (2008). Notch signaling regulates platelet-derived growth factor receptor-beta expression in vascular smooth muscle cells. *Circ. Res.* **102**, 1483-1491.
Lafleur, M. A., Forsyth, P. A., Atkinson, S. J., Murphy, G. and Edwards, D. R. (2001). Perivascular cells regulate endothelial membrane type-1 matrix metalloproteinase activity. *Biochem. Biophys. Res. Commun.* **282**, 463-473.
Liu, H., Kennard, S. and Lilly, B. (2009). NOTCH3 expression is induced in mural cells through an autoregulatory loop that requires endothelial-expressed JAGGED1. *Circ. Res.* **104**, 466-475.
Montell, D. J. (2008). Morphogenetic cell movements: diversity from modular mechanical properties. *Science* **322**, 1502-1505.
Murakami, T., Suzuma, K., Takagi, H., Kita, M., Ohashi, H., Watanabe, D., Ojima, T., Kurimoto, M., Kimura, T., Sakamoto, A. et al. (2006). Time-lapse imaging of vitreoretinal angiogenesis originating from both quiescent and mature vessels in a novel ex vivo system. *Invest. Ophthalmol. Vis. Sci.* **47**, 5529-5536.
Nishiyama, K., Takaji, K., Kataoka, K., Kurihara, Y., Yoshimura, M., Kato, A., Ogawa, H. and Kurihara, H. (2005). Id1 gene transfer confers angiogenic property on fully differentiated endothelial cells and contributes to therapeutic angiogenesis. *Circulation* **112**, 2840-2850.
Noguera-Troise, I., Daly, C., Papadopoulos, N. J., Coetzee, S., Boland, P., Gale, N. W., Lin, H. C., Yancopoulos, G. D. and Thurston, G. (2006). Blockade of Dll4 inhibits tumour growth by promoting non-productive angiogenesis. *Nature* **444**, 1032-1037.
Ozerdem, U. and Stallcup, W. B. (2003). Early contribution of pericytes to angiogenic sprouting and tube formation. *Angiogenesis* **6**, 241-249.
Ozerdem, U., Grako, K. A., Dahlin-Huppe, K., Monosov, E. and Stallcup, W. B. (2001). NG2 proteoglycan is expressed exclusively by mural cells during vascular morphogenesis. *Dev. Dyn.* **222**, 218-227.

Perryn, E. D., Czirok, A. and Little, C. D. (2008). Vascular sprout formation entails tissue deformations and VE-cadherin-dependent cell-autonomous motility. *Dev. Biol.* **313**, 545-555.
Phng, L. K. and Gerhardt, H. (2009). Angiogenesis: a team effort coordinated by notch. *Dev. Cell* **16**, 196-208.
Provis, J. M., Leech, J., Diaz, C. M., Penfold, P. L., Stone, J. and Keshet, E. (1997). Development of the human retinal vasculature: cellular relations and VEGF expression. *Exp. Eye Res.* **65**, 555-568.
Ridgway, J., Zhang, G., Wu, Y., Stawicki, S., Liang, W. C., Chanthery, Y., Kowalski, J., Watts, R. J., Callahan, C., Kasman, I. et al. (2006). Inhibition of Dll4 signalling inhibits tumour growth by deregulating angiogenesis. *Nature* **444**, 1083-1087.
Schmidt, M., Paes, K., De Maziere, A., Smyczek, T., Yang, S., Gray, A., French, D., Kasman, I., Klumperman, J., Rice, D. S. et al. (2007). EGFL7 regulates the collective migration of endothelial cells by restricting their spatial distribution. *Development* **134**, 2913-2923.
Siekmann, A. F. and Lawson, N. D. (2007). Notch signalling limits angiogenic cell behaviour in developing zebrafish arteries. *Nature* **445**, 781-784.
Stone, J., Itin, A., Alon, T., Pe'er, J., Gnessin, H., Chan-Ling, T. and Keshet, E. (1995). Development of retinal vasculature is mediated by hypoxia-induced vascular endothelial growth factor (VEGF) expression by neuroglia. *J. Neurosci.* **15**, 4738-4747.
Suchting, S., Freitas, C., le Noble, F., Benedito, R., Breant, C., Duarte, A. and Eichmann, A. (2007). The Notch ligand Delta-like 4 negatively regulates endothelial tip cell formation and vessel branching. *Proc. Natl. Acad. Sci. USA* **104**, 3225-3230.
Theveneau, E., Marchant, L., Kuriyama, S., Gull, M., Moepps, B., Parsons, M. and Mayor, R. (2010). Collective chemotaxis requires contact-dependent cell polarity. *Dev. Cell* **19**, 39-53.
Uemura, A., Ogawa, M., Hirashima, M., Fujiwara, T., Koyama, S., Takagi, H., Honda, Y., Wiegand, S. J., Yancopoulos, G. D. and Nishikawa, S. (2002). Recombinant angiopoietin-1 restores higher-order architecture of growing blood vessels in mice in the absence of mural cells. *J. Clin. Invest.* **110**, 1619-1628.
van Hinsbergh, V. W. and Koolwijk, P. (2008). Endothelial sprouting and angiogenesis: matrix metalloproteinases in the lead. *Cardiovasc. Res.* **78**, 203-212.
Vitorino, P. and Meyer, T. (2008). Modular control of endothelial sheet migration. *Genes Dev.* **22**, 3268-3281.
Williams, C. K., Li, J. L., Murga, M., Harris, A. L. and Tosato, G. (2006). Up-regulation of the Notch ligand Delta-like 4 inhibits VEGF-induced endothelial cell function. *Blood* **107**, 931-939.
Yamanda, S., Ebihara, S., Asada, M., Okazaki, T., Niu, K., Ebihara, T., Koyanagi, A., Yamaguchi, N., Yagita, H. and Arai, H. (2009). Role of ephrinB2 in nonproductive angiogenesis induced by Delta-like 4 blockade. *Blood* **113**, 3631-3639.
Yamashita, J., Itoh, H., Hirashima, M., Ogawa, M., Nishikawa, S., Yurugi, T., Naito, M. and Nakao, K. (2000). Flk1-positive cells derived from embryonic stem cells serve as vascular progenitors. *Nature* **408**, 92-96.

Angiogenic morphogenesis driven by dynamic and heterogeneous collective endothelial cell movement

DEV068023 Supplementary Material

Files in this Data Supplement:

Supplemental Table S1 -

Supplemental Figure S1 -

Fig. S1. Selective marking of ECs by staining with SYTO dyes. (A,B) Serial confocal images along the z-axis (A) and a z-stack image (B) of live cells immunostained for CD31 and PDGFRß with nuclear SYTO dye staining in a murine aortic ring assay. ECs (CD31+) were more strongly stained with SYTO-16 than were MCs (CD31- PDGFRß+). (C) Distinct localization of SYTO-61 and Ednra-EGFP signals in a murine aortic ring assay using Ednraegfp mouse. EGFP signals are detected only in CD31- MCs (asterisks) (see also Movie 2 in the supplementary material). (D) Flow cytometry analysis showing preferential SYTO-61 staining for CD31+, Ednra-EGFP− ECs. Scale bars: 25 μm.

Supplemental Figure S2 -

Fig. S2. The percentage of ECs undergoing mitosis in in vitro and in vivo angiogenesis. (A) An example of ECs undergoing mitosis observed in time-lapse live imaging of a murine aortic ring assay. Nuclei were stained with SYTO-16 dye. Red arrows indicate an event of mitosis. (B) Mitotic ECs were detected by staining for PH3 in a murine aortic ring assay and murine retinal neovessels at P1 and P3. The rate of PH3+ ECs to total ECs was quite low equally among the three groups. (C) The rate of PH3+ ECs was compared between distal and proximal regions. PH3+ ECs (arrows) were detected more frequently in the distal region, including the tip, than in more proximal regions in a murine aortic ring assay, as well as in murine retinal angiogenesis. Solid and broken lines indicate subareas referred to as □distal 400□ and □proximal□, respectively.

Supplemental Figure S3 -

Fig. S3. An example of the trajectory analysis. Trajectory of the EC indicated by red arrows in Fig. 2A is shown. Nuclear positions were orthogonally projected to the axis of elongation (white arrow), which corresponds to the direction of the tip migration. The vertical axis is the position of each cell (pixels) and the horizontal axis is time (minutes). Zero position of the vertical axis indicates the position of the base of the branch. The trajectory of the tip was drawn in thick black. Using the nuclear coordinates extracted from confocal images obtained by tracking the cell nuclei, a trajectory of the individual cell can be re-drawn in an elongating branch. The EC (yellow trajectory) migrates to the